FOURTH REVISED MS 23/09/2020

Impact of the novel Z-acceptor ligand bis{(ortho-diphenylphosphino)phenyl}zinc (ZnPhos) on the formation and reactivity of low-coordinate Ru(0) centers

Fedor M. Miloserdov,* Connie J. Isaac, Madeleine L. Beck, Arron L. Burnage, James C. B. Farmer, Stuart A Macgregor,* Mary F. Mahon, and Michael K. Whittlesey*

Corresponding Authors

Fedor M. Miloserdov − Department of Chemistry, University of Bath, Bath BA2 3QD, U.K.; orcid.org/0000-0001-6420-211X; E-mail: fm593@bath.ac.uk

Stuart A. Macgregor − Institute of Chemical Sciences, School of Engineering and Physical Sciences, Heriot-Watt University, Edinburgh EH14 4AS, U.K.; orcid.org/ 0000-0003-3454-6776; E-mail: s.a.macgregor@hw.ac.uk

Michael K. Whittlesey − Department of Chemistry, University of Bath, Bath BA2 3QD, U.K.; orcid.org/0000-0002-5082-3203; E-mail: m.k.whittlesey@bath.ac.uk

Authors

Connie J. Isaac − Department of Chemistry, University of Bath, Bath BA2 3QD, U.K.

Madeleine L. Beck − Department of Chemistry, University of Bath, Bath BA2 3QD, U.K.

Arron L. Burnage − Institute of Chemical Sciences, School of Engineering and Physical Sciences, Heriot-Watt University, Edinburgh EH14 4AS, U.K.

James C. B. Farmer − Institute of Chemical Sciences, School of Engineering and Physical Sciences, Heriot-Watt University, Edinburgh EH14 4AS, U.K.

Mary F. Mahon − Department of Chemistry, University of Bath, Bath, BA2 3QD, U.K.

Abstract

The preparation and reactivity with H_2 of two Ru complexes of the novel ZnPhos ligand (ZnPhos = $Zn(o\text{-}C_6H_4PPh_2)_2$) are described. $Ru(ZnPhos)(CO)_3$ (**2**) and $Ru(ZnPhos)(IMe_4)_2$ (**4**; IMe_4 = 1,3,4,5-tetramethylimidazol-2-ylidene) are formed directly from the reaction of $Ru(PPh_3)(C_6H_4PPh_2)_2(ZnMe)_2$ (**1**) or $Ru(PPh_3)_3HCl/LiCH_2TMS/ZnMe_2$ with CO and IMe_4, respectively. Structural and electronic structure analyses characterize both **2** and **4** as Ru(0) species in which Ru donates to the Z-type Zn center of the ZnPhos ligand; in **2**, Ru adopts an octahedral coordination, while **4** displays square-pyramidal coordination with Zn in the axial position. Under photolytic conditions **2** loses CO to give $Ru(ZnPhos)(CO)_2$ that then adds H_2 over the Ru-Zn bond to form $Ru(ZnPhos)(CO)_2(\mu\text{-}H)_2$ (**3**). In contrast, **4** reacts directly with H_2 to set up an equilibrium with $Ru(ZnPhos)(IMe_4)_2H_2$ (**5**), the product of oxidative addition at the Ru center. DFT calculations rationalize these different outcomes in terms of the energies of the square-pyramidal $Ru(ZnPhos)L_2$ intermediates in which Zn sits in a basal site: for L = CO this is readily accessed and allows H_2 to add across the Ru-Zn bond, but for L = IMe_4 this species is kinetically inaccessible and reaction can only occur at the Ru center. This difference is related to the strong π-acceptor ability of CO compared to IMe_4. Steric effects associated with the larger IMe_4 ligands are not significant. Species **4** can be considered as a $Ru(0)L_4$ species that is stabilized by the Ru→Zn interaction. As such it is a rare example of a stable $Ru(0)L_4$ species devoid of strong π-acceptor ligands.

Introduction

The classification of donor ligands as either L- or X-type is well-established in organometallic chemistry.[1] A third, less developed class are Z-type ligands which, in contrast to the donor behavior of the first two groups, act as σ-acceptors to transition metals (TM→Z) as a result of the Lewis acidic nature of Z.[2-4] One approach that has proven popular in recent years for the development of new TM→Z interactions has been to entrap the Lewis acid within a scaffold of bi- or tridentate L donors.[5-25] This has afforded not only interesting stoichiometric reactivity with small molecules, exemplified by the Pt→Sb[16] and Ni→Ga[18] complexes shown in Scheme 1a and 1b, but also facilitated high levels of catalytic activity. One such case is the extremely efficient Pd→Al catalyst for CO_2 hydrosilylation shown in Scheme 1c.[23]

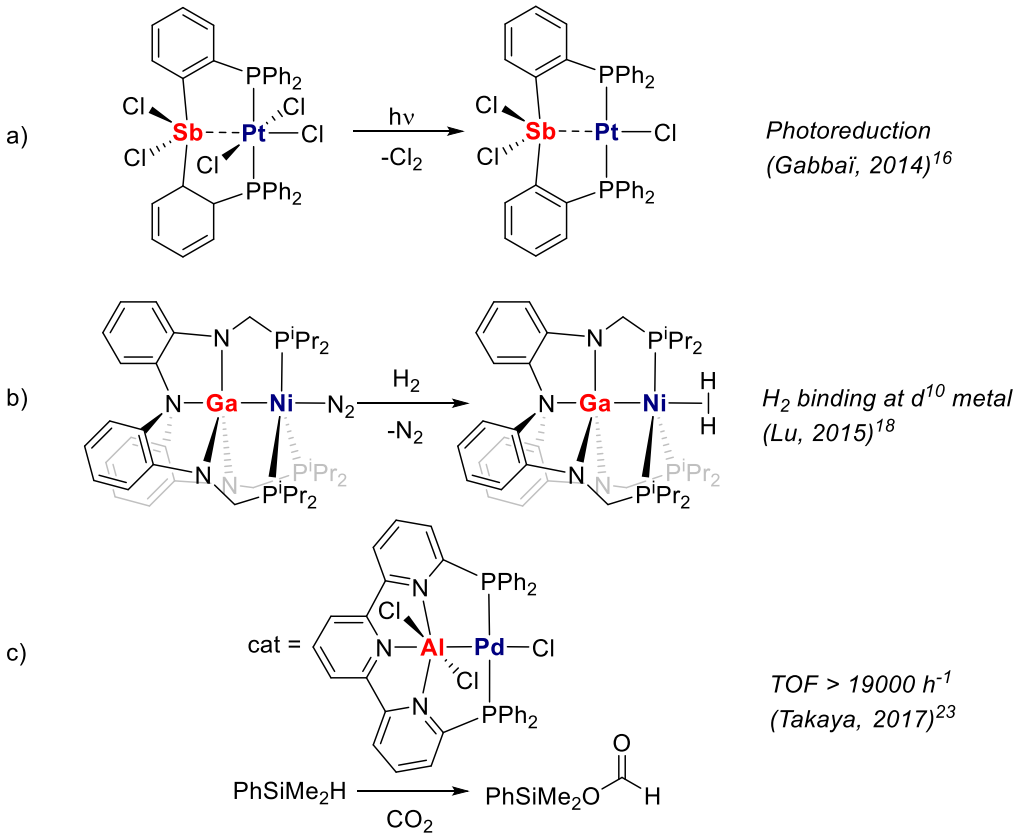

Scheme 1 Representative examples of scaffold-supported Z-type ligands

The bis-(ortho-phosphinophenyl) moiety[26] featured in Scheme 1a has proven to be particularly useful in stabilizing Z-type ligands from group 13 (B, Al, Ga, In),[10, 12, 14, 27-32] as well as those containing elements from further to the right in the *p*-block (Sn, Sb, Te, Bi).[9, 16, 20, 24, 33-35] In marked contrast to this array of ligands, analogues featuring elements from group 12 are limited to only the mercury derivative, $Hg(o\text{-}C_6H_4PPh_2)_2$.[36-39] The Bennett group has employed this ligand for the preparation of a small number of Pd→Hg and Pt→Hg derivatives, although there have been no reports on their reactivity towards small molecules. We now report the in-situ generation of the zinc derivative, $Zn(o\text{-}C_6H_4PPh_2)_2$ (which we refer to as ZnPhos, the zinc analogue of the well-known DPEphos ligand) during the formation of two ruthenium complexes, $Ru(ZnPhos)(CO)_3$ (**2**) and $Ru(ZnPhos)(IMe_4)_2$ (**4**; IMe_4 = 1,3,4,5-tetramethylimidazol-2-ylidene). Both complexes react with H_2; the former upon photolysis to afford a product arising from H_2 addition across the Ru-Zn bond, the latter with reversible addition at Ru. DFT studies have been used to rationalize these outcomes in terms of the different impact of the ligands, L, on the electronic structure and geometries that are accessible to the reacting $Ru(ZnPhos)L_2$ species (L = CO and IMe_4).

Experimental

General Comments. All manipulations were carried out at room temperature under argon using standard Schlenk, high vacuum and glovebox techniques using dry and degassed solvents. C_6H_5F was additionally dried over $LiAlH_4$ before use. C_6D_6 and THF-d_8 were vacuum transferred from potassium. NMR spectra were recorded at 298 K (unless otherwise stated) on Bruker Avance 400 and 500 MHz NMR spectrometers and referenced as follows: C_6D_6 (^{1}H, δ 7.16; ^{13}C, δ 128.0), THF-d_8 (^{1}H, δ 1.72; ^{13}C, δ 25.3). $^{31}P\{^1H\}$ spectra were referenced externally to 85% H_3PO_4 (δ 0.0). UV-Vis spectra were recorded on a Cary 60 spectrometer. IR spectra were recorded in $C_6D_5CD_3$ solution on a Nicolet Nexus

spectrometer. Elemental analyses were performed by Elemental Microanalysis Ltd, Okehampton, Devon, U.K. $Ru(PPh_3)_3HCl$·toluene, $Ru(PPh_3)(C_6H_4PPh_2)_2H(ZnMe)$·THF, $Ru(PPh_3)_2(CO)_3$ and IMe_4, were prepared according to literature methods.[40-42] Prior to use, $Ru(PPh_3)_3HCl$·toluene was dried under high vacuum and ground to a fine powder affording a material with *ca.* 0.8 molecules of toluene per Ru (on the basis of the ^1H NMR spectrum). $LiCH_2TMS$ was used in the form of a colorless solid obtained after cooling a commercial 1.0 M solution in pentane at -32 ºC, separating the resulting colorless crystals by decantation and drying under vacuum.

$Ru(PPh_3)(C_6H_4PPh_2)_2(ZnMe)_2$ (1). $ZnMe_2$ (0.75 mL of 2.0 M toluene solution, 1.5 mmol, 10 equiv) was added to a suspension of $Ru(PPh_3)(C_6H_4PPh_2)_2H(ZnMe)$·THF (156 mg, 0.15 mmol) in toluene (0.75 mL) and the suspension stirred at 60 ºC for 3 h in an ampule fitted with a J. Youngs resealable tap. The resulting dark yellow/brown solution was filtered through a pad of Celite® and washed with hexane (0.5 mL). The combined filtrate and washings were treated with hexane (4.5 mL) and left to crystallize at room temperature for 15 h and then at -32 ºC for 4 h. Yellow-orange crystals were separated, washed with hexane (2 x 3 mL) and dried under vacuum. Yield: 149 mg (81%, contains ca. 10 mol% of toluene and hexane based on ^1H NMR). **1** exists in solution as a mixture of mer- and fac-isomers in a ca. 20:1 ratio with mer-**1** being the major species. mer-**1**. ^1H NMR (500 MHz, C_6D_6): δ 8.26 (dd, J = 10.1, 7.6 Hz, 2H, $PPh_2C_6H_4$), 7.99 (dd, J = 10.4, 7.4 Hz, 2H, $PPh_2C_6H_4$), 7.45 (ddd, J = 9.7, 6.5, 3.0 Hz, 6H, PPh_3), 7.21 (t, J = 7.5, 2H, $PPh_2C_6H_4$), 7.18-6.62 (m, 27H, $PPh_2C_6H_4$, PPh_3), 6.47 (td, J = 7.9, 2.1 Hz, 2H, $PPh_2C_6H_4$), 6.35 (t, J = 9.0 Hz, 2H, $PPh_2C_6H_4$), 0.43 (s, 3H, $ZnCH_3$), -0.91 (s, 3H, $ZnCH_3$). $^{31}P\{^1H\}$ NMR (202 MHz, C_6D_6): δ 51.1 (dd, $^2J_{PP}$ = 265, 23 Hz, PPh_3), -25.5 (t, $^2J_{PP}$ = 24 Hz, $PPh_2C_6H_4$ (cis to PPh_3)), -25.8 (dd, $^2J_{PP}$ = 265, 25 Hz, $PPh_2C_6H_4$ (trans to PPh_3)).$^{13}C\{^1H\}$ NMR (101 MHz, C_6D_6): δ 176.4 (td, J_{CP} = 12, 8 Hz, Ru-$C_{metalated}$), 157.8 (dd, J_{CP} = 48, 6 Hz, C_{ipso}-$P_{metalated}$), 155.7 (dd, J_{CP} = 48, 8 Hz, C_{ipso}-$P_{metalated}$),

153.0 (dd, J_{CP} = 49, 2 Hz, C_{ipso}-$P_{metalated}$), 140.9 (ddd, J_{CP} = 18, 4, 3 Hz), 139.9-139.3 (m, including C_{ipso}-PPh_3), 138.5 (d, J_{CP} = 24 Hz, C_{ipso}-$P_{metalated}$), 134.3 (d, J_{CP} = 10 Hz), 134.0 (dd, J_{CP} = 11, 1 Hz), 132.8-132.3 (m), 132.1 (d, J_{CP} = 10 Hz), 130.4 (vt, J = 3 Hz), 130.3 (d, J_{CP} = 3 Hz), 130.1 (d, J_{CP} = 2 Hz), 128.9 (d, J_{CP} = 2 Hz), 128.8 (d, J_{CP} = 2 Hz), 128.6 -128.4 (m), 128.3-127.6 (m, overlapped with C_6D_6), 127.3 (d, J_{CP} = 9 Hz), 127.2 (s), 126.8 (d, J_{CP} = 9 Hz), 124.7 (d, J_{CP} = 9 Hz), 122.3 (d, J_{CP} = 8 Hz), 9.8 (s, $ZnCH_3$), -4.5 (s, $ZnCH_3$). fac-**1**. Selected ^{1}H NMR (500 MHz, C_6D_6): δ 8.11-8.05 (m, 1H, $PPh_2C_6H_4$), 7.63 (t, J = 8.9 Hz, 2H, $PPh_2C_6H_4$), 7.51 (ddd, J = 10.1, 6.8, 3.1 Hz, 6H, PPh_3), 7.36-7.30 (m, 2H, $PPh_2C_6H_4$), 6.59 (t, J = 7.7, 2H, $PPh_2C_6H_4$), 6.52 (t, J = 7.7 Hz, 1H, $PPh_2C_6H_4$), -0.42 (s, 6H, $ZnCH_3$). ^{31}P{^{1}H} NMR (202 MHz, C_6D_6): 39.7 (dd, $^2J_{PP}$ = 22, 18 Hz, PPh_3), -30.9 (t, $^2J_{PP}$ = 18 Hz, $PPh_2C_6H_4$), -34.8 (t, $^2J_{PP}$ = 22 Hz, $PPh_2C_6H_4$). Selected ^{13}C{^{1}H} NMR (101 MHz, C_6D_6): δ -2.6 (s, $ZnCH_3$; confirmed by HSQC). Anal. Found: C, 64.58; H, 4.83; Calcd. for $C_{56}H_{49}P_3RuZn_2$: C, 64.26; H, 4.72; Calcd. for $C_{56}H_{49}P_3RuZn_2 \cdot 0.1C_6H_5CH_3 \cdot 0.1C_6H_{14}$: C, 64.65; H, 4.85 (NMR spectroscopy confirmed the presence of toluene and hexane; Figure S2).

Ru(ZnPhos)(CO)$_3$ (2). A C_6H_5F solution (2 mL) of $Ru(PPh_3)_3HCl \cdot$toluene (300 mg, 0.3 mmol) and $LiCH_2TMS$ (56 mg, 0.6 mmol, 2 equiv) was stirred for 5 min in a J. Young's ampule to form an orange suspension. Additional $Ru(PPh_3)_3HCl \cdot$toluene (300 mg, 0.3 mmol), together with $ZnMe_2$ (3 mL, 2.0 M solution in toluene, 10 equiv) and C_6H_5F (2 mL) were then added. The red solution was stirred for 3 h at 60 °C, resulting in a yellow-brown solution. After cooling, the solution was freeze-pump-thaw degassed, placed under an atmosphere of CO and stirred again at 60 °C for 2 h. Solvents and excess $ZnMe_2$ were collected by vacuum into a cold trap and quenched. Benzene (6 mL) was added to afford a precipitate of LiCl. The suspension was filtered, the residue washed with C_6H_6 (2 mL) and the combined filtrate and washings treated with hexane (8 mL) to yield yellow crystals over 24 h. These were isolated by filtration, washed with Et_2O (5 mL) and dried under vacuum.

Yield: 300 mg (63%). Alternatively, **2** could be obtained in > 95% NMR yield by reaction of **1** (10 mg, 0.01 mmol) with CO (1 atm) in C_6D_6 (0.5 mL) over 30 min at 60 °C. ^{1}H NMR (500 MHz, C_6D_6): δ 8.33 (d, *J* = 6.9 Hz, 2H, PC_6H_4Zn), 7.70- 7.66 (m, 8H, PPh_2), 7.60- 7.57 (m, 2H, PC_6H_4Zn), 7.33 (t, *J* = 7.0 Hz, 2H, PC_6H_4Zn), 7.02 (t, *J* = 7.5 Hz, 2H, PC_6H_4Zn), 6.96-6.91 (m, 12H, PPh_2). $^{31}P\{^1H\}$ NMR (202 MHz, C_6D_6): δ 60.9 (s). $^{13}C\{^1H\}$ NMR (126 MHz, C_6D_6): δ 203.9 (t, $^2J_{CP}$ = 15 Hz, Ru-CO), 201.9 (t, $^2J_{CP}$ = 6 Hz, Ru-CO), 171.5 (vt, *J* = 30 Hz, PC_6H_4Zn), 146.0 (vt, *J* = 32 Hz, PPh_2), 139.6 (vt, *J* = 13 Hz, PC_6H_4Zn), 138.4 (vt, *J* = 22 Hz, PC_6H_4Zn), 133.0 (vt, *J* = 5 Hz, PPh_2), 130.0 (s, PPh_2), 129.0 (s, PC_6H_4Zn), 128.7-128.5 (m, PC_6H_4Zn and PPh_2), 126.1 (s, PC_6H_4Zn). IR ($C_6D_5CD_3$, cm^{-1}): 2012 (ν_{CO}), 1959 (ν_{CO}), 1931 (ν_{CO}). Anal. Found: C, 61.37; H, 3.94. Calcd. for $C_{39}H_{28}O_3P_2RuZn{\cdot}0.25C_6H_6{\cdot}0.10Et_2O$: C, 61.41; H, 3.87 (NMR spectroscopy confirmed the presence of benzene and Et_2O; Figure S5).

Ru(ZnPhos)(^{13}CO)$_3$ (2*). As for **2** but using $Ru(PPh_3)_3HCl{\cdot}$toluene (150 mg, 0.15 mmol), $LiCH_2TMS$ (28 mg, 0.3 mmol, 2 equiv) in C_6H_5F (1 mL), followed by $Ru(PPh_3)_3HCl{\cdot}$toluene (150 mg, 0.15 mmol), $ZnMe_2$ (1.5 mL, 2.0 M solution in toluene, 10 equiv) and C_6H_5F (1 mL) under atmosphere of ^{13}CO to give 96 mg (41%) **2***. $^{31}P\{^1H\}$ NMR (202 MHz, C_6D_6): δ 60.9 (m).

Ru(ZnPhos)(CO)$_2$(μ-H)$_2$ (3). (i) Via photolysis of **2** with H_2: **2** (6 mg, 0.007 mmol) and THF-d_8 (0.5 mL) were charged to a J. Young's resealable NMR tube, the sample freeze-pump-thaw degassed (3 cycles) and 1 atm of H_2 (or D_2 for formation of $Ru(ZnPhos)(CO)_2(\mu\text{-}D)_2$ for IR analysis; see below) added. The reaction mixture was photolyzed with a 500W Hg arc lamp at ca. 0 °C, leading to full conversion of the starting material to two new products over 8 h (comparable photochemical behavior was observed in C_6D_6). The major species was assigned as $Ru(ZnPhos)(CO)_2(\mu\text{-}H)_2$ (**3**), the minor species as $Ru(PPh_3)_2(CO)_2H_2$.[43] The solution was concentrated and layered with hexane to yield a very small amount of light-yellow plate like crystals of **3**, together with amorphous yellow solid, over 24 h. The

combination of a low yield and presence of $Ru(PPh_3)_2(CO)_2H_2$ prevented elemental analysis for **3**. Selected ^{1}H NMR (500 MHz, THF-d_8): δ -7.61 (t, $^2J_{HP}$ = 17.0 Hz, 2H, RuH). $^{31}P\{^1H\}$ NMR (202 MHz, THF-d_8): δ 59.3 (s). ^{1}H NMR (500 MHz, C_6D_6) δ -7.25 (t, $^2J_{HP}$ = 17.0 Hz, 2H, RuH). $^{31}P\{^1H\}$ NMR (202 MHz, C_6D_6): δ 61.2 (s). IR (C_6D_6, cm^{-1}): 2041 (ν_{CO}), 1998 (ν_{CO}), 1898 (ν_{RuH}); Ru(ZnPhos)$(CO)_2(\mu\text{-}D)_2$: 2038 (ν_{CO}), 1989 (ν_{CO}). (ii) Via photolysis of **2** with $NH_3{\cdot}BH_3$ and $Me_2NH{\cdot}BH_3$*:* J. Youngs resealable NMR tubes containing C_6D_6 solutions (0.5 mL) of **2** (6 mg, 0.007 mmol) and $H_3N{\cdot}BH_3$ (2 mg, 0.07 mmol) or $Me_2NH{\cdot}BH_3$ (4 mg, 0.07 mmol) were photolyzed for 6 and 8 h respectively (at ca. 5 C) to afford **3**, together with $Ru(PPh_3)_2(CO)_2H_2$. Comparable reactivity was seen in THF-d_8. The major boron-containing product of the reaction with $Me_2NH{\cdot}BH_3$ was $[Me_2N\text{-}BH_2]_2$ (^{11}B NMR (128 MHz**,** C_6D_6): δ 5.3, t, $^1J_{BH}$ = 112 Hz).[44]

Ru(ZnPhos)(^{13}CO)$_2$(μ-H)$_2$ (3*). A J. Young's resealable NMR tube was charged with **2*** (6 mg, 0.007 mmol) and THF-d_8 (0.5 mL), placed under 1 atm of H_2 and photolyzed at 0 °C for 4 h to afford **3***, which was spectroscopically characterized. Selected ^{1}H NMR (400 MHz, THF-d_8) δ -7.61 (m, 2H). Selected ^{1}H NMR (400 MHz, THF-d_8): δ -7.61 (m, 2H). $^{31}P\{^1H\}$ NMR (162 MHz, THF-d_8): δ 59.5 (t, $^2J_{CP}$ = 8 Hz). Selected $^{13}C\{^1H\}$ NMR (101 MHz, THF-d_8): δ 198.9 (t, $^2J_{CP}$ = 7.5 Hz).

Ru(ZnPhos)(IMe$_4$)$_2$ (4). To an agitated suspension of $Ru(PPh_3)_3HCl{\cdot}$toluene (150 mg, 0.15 mmol) in C_6H_5F (1.5 mL) was added $LiCH_2TMS$ (28 mg, 0.30 mmol). After 5 min, all of the purple starting material had dissolved to give an orange suspension, which was treated with $ZnMe_2$ (1.5 mL of 2.0 M toluene solution, 3.0 mmol) before a second portion of $Ru(PPh_3)_3HCl{\cdot}$toluene (150 mg, 0.15 mmol) was added. The resulting red solution was freeze-pump-thaw degassed, sealed under vacuum in a J. Youngs resealable ampule and the mixture heated at 60 ^{o}C for 3 h. The yellow-brown reaction mixture was cooled, cannula filtered, and the residual LiCl washed with benzene (1 mL). The combined filtrate and

washings were concentrated under vacuum and volatile $ZnMe_2$ and solvents collected in a cold trap and quenched. The residual yellow brown oil was redissolved in benzene (5 mL) and IMe_4 (187 mg, 1.5 mmol) added. The resulting red solution was stirred for 20 h, and then filtered through a pad of Celite®, which was washed with benzene (3 mL). The combined filtrate and benzene washings were treated with hexane (8 mL) and left to crystallize at room temperature (3 h), and then at -20 ºC (24 h). The product **4** crystallized as dark red blocks, together with light yellow blocks of $(IMe_4)_2ZnMe_2$ (Figure S25), which were separated from the mother liqor (**A**). An initial batch of **4** was isolated upon extraction of the solid red material with Et_2O, evaporation and crystallization of the residue from benzene-hexane (1:1), giving 75 mg of **4** as dark red-colored crystalline solid after drying under vacuum. A second batch (70 mg) was obtained by evaporation of **A** and crystallization of the residue, again from benzene-hexane (1:1). Yield 145 mg (47%; contains 1.5 molecules of C_6H_6). Alternatively, **4** could be obtained in ca. 90% NMR yield by reaction of **1** (10.5 mg, 0.01 mmol) with IMe_4 (10 mg, 8 equiv) in C_6D_6 (0.5 mL) over 3 h. ^{1}H NMR (400 MHz, THF-d_8): δ 8.08 (ddd, J = 6.9, 1.5, 0.7 Hz, 2H, PC_6H_4Zn), 7.07 (tq, J = 7.1, 1.3 Hz, 2H, PC_6H_4Zn), 6.98-6.90 (m, 4H, $P(C_6H_5)_2$), 6.87 (dt, J = 6.4, 2.9 Hz, 2H, PC_6H_4Zn), 6.84-6.78 (m, 16H, PPh_2), 6.72 (tq, J = 7.4, 1.3 Hz, 2H, PC_6H_4Zn), 3.09 (s, 6H, NCH_3), 2.45 (s, 6H, NCH_3), 1.74 (s, 6H, H_3CC=CCH_3, overlapped with residual solvent signal of THF-d_8), 1.50 (s, 6H, H_3CC=CCH_3). ^{31}P{^{1}H} NMR (202 MHz, THF-d_8): δ 56.3 (s). ^{13}C{^{1}H} NMR (126 MHz, THF-d_8): δ 198.5 (t, $^2J_{CP}$ = 14 Hz, RuC_{NHC}), 176.7 (vt, J = 37 Hz, PC_6H_4Zn), 154.4 (vt, J = 30 Hz, PC_6H_4Zn), 144.6 (vt, J = 9 Hz, PPh_2), 137.0 (vt, J = 14 Hz, PC_6H_4Zn), 132.9-132.6 (m, PPh_2 and PC_6H_4Zn), 126.8 (vt, J = 3 Hz, PPh_2), 126.53 (s, PPh_2), 126.48 (s, PC_6H_4Zn), 124.2 (s, NC=CN), 123.9 (s, NC=CN), 123.0 (s, PC_6H_4Zn), 34.8 (s, NCH_3), 33.8 (s, NCH_3), 9.6 (s, H_3CC=CCH$_3$), 8.6 (s, H_3CC=CCH$_3$). UV-Vis (C_6H_6; λ_{max} (nm)): 365 (sh), 460, 555 (sh).

Anal. Found: C, 67.54; H, 5.91; N, 5.42. Calcd. for $C_{50}H_{52}N_4P_2RuZn \cdot 1.5C_6H_6$: C, 67.20; H, 5.83; N, 5.31 (NMR spectroscopy confirmed the presence of benzene; Figure S21).

Ru(ZnPhos)(IMe$_4$)$_2$H$_2$ (5). A J. Young's resealable NMR tube was charged with a THF-d_8 (0.5 mL) solution of **4** (9.5mg, 0.01 mmol) and placed under 1 atm of H_2. ^{1}H and ^{31}P{^{1}H} NMR spectra showed the immediate formation of Ru(ZnPhos)(IMe$_4$)$_2$H$_2$ **5** in equilibrium with **4** (Table S1). ^{1}H NMR (400 MHz, THF-d_8): δ 8.35 (d, J = 6.8 Hz, 2H, PC_6H_4Zn), 7.25 (br t, J = 7.3 Hz, 2H, PC_6H_4Zn), 3.51 (s, 6H, NCH_3), 2.71 (s, 6H, NCH_3), 1.75 (s, 6H, CCH_3), 1.41 (s, 6H, CCH_3), -6.57 (m, 2H, Ru*H*). ^{31}P{^{1}H} NMR (162 MHz, THF-d_8): δ 83.4 (s). Selected ^{13}C{^{1}H} NMR (101 MHz, THF-d_8, 211 K): δ 191.2 (t, $^2J_{CP}$ = 9 Hz, RuC_{NHC}).

Crystallographic Details. Data were obtained using an Agilent SuperNova instrument and a Cu-Kα source. All experiments were conducted at 150 K. The structures were solved using SHELXT[45] and refined using SHELXL[46] via the Olex2[47] interface. Refinements were generally uneventful, and only points of particular note will be detailed hereafter. The asymmetric unit in the structure in **1** contains two independent molecules (see Supporting Information). One guest molecule of benzene accompanies one molecule of the bimetallic complex in the asymmetric unit of **2**. Meanwhile, the asymmetric unit in **3** equates to one pair of the ruthenium–zinc containing complexes and a pair of THF molecules. The guest solvent was entirely ordered, while one carbon in the ligated THF ligand present in each of the complexes was disordered over 2 sites in a 46:54 ratio. The disorder model refined well upon inclusion of some distance and ADP restraints. Refinement also took account of some racemic twinning (36%) about the *b* axis. A combination of twinning and residual electron density rendered it difficult to locate and refine the hydride ligands. However, a credible convergence was achieved for H1B and H2B in the molecule based on Ru1B - albeit with separate, similarity distance restraints imposed upon the two Ru-H bonds

and the Zn-H distances therein. In the case of the molecule based on Ru1A, it was not possible to locate the hydrides with any certainty in terms of the electron density, so these were omitted from the refinement (Figure 1). The asymmetric unit in **4** contains half of a complex molecule and one molecule of benzene. The remainder of the main feature is generated *via* the crystallographic rotation axis that is co-incident with the two metal centers. Crystallographic data for all compounds has been deposited with the Cambridge Crystallographic Data Centre as supplementary publications CCDC 2031254 for **1** (Supporting Information), CCDC 1995946-1995948 for **2**, **3**, and **4**, respectively, and CCDC 2003689 for $(IMe_4)_2ZnMe_2$ (Supporting Information). Copies of these data can be obtained free of charge on application to CCDC, 12 Union Road, Cambridge CB2 1EZ, UK: fax(+44) 1223 336033, e-mail: deposit@ccdc.cam.ac.uk.

Computational Details. DFT calculations were run with Gaussian 09 (Revision D.01).[48] Geometry optimizations and thermodynamic corrections were performed with the BP86 functional[49, 50] with Ru, Zn and P centers described by Stuttgart RECPs and associated basis sets[51] and 6-31G** basis sets for all other atoms.[52, 53] A set of d-orbital polarization functions was added to P ($\zeta^d = 0.387$).[54] All stationary points were fully characterized via analytical frequency calculations as either minima (all positive frequencies) or transition states (one negative frequency) and the latter were characterized via IRC calculations and subsequent geometry optimizations to confirm the adjacent minima. Key stationary points were subjected to conformational searching using our published protocol[55] and the lowest energy conformers reported. Electronic energies were recomputed with the ωB97x-D functional[56] using def2-TZVP basis sets[57, 58] and a correction for benzene solvent (PCM approach).[59] This protocol was previously successful in reproducing the relative free energies of range of Ru-Zn heterobimetallic complexes in solution.[41] Details of all computed structures are provided in the Supporting Information.

Electronic structure analyses on **2**, **3** and **4** employed geometries derived from the crystallographic studies with the H atom positions optimized. For **3**, of the two molecules in the asymmetric unit, that based on Ru1B was used as, unlike the molecule based on Ru1A, it contained a credible inclusion of the hydrides; the THF molecule was also removed. Fully optimized geometries were employed for other species where crystallographic data were not available. Quantum theory of atoms in molecules (QTAIM)[60] employed the AIMALL package,[61] with core electrons on Ru, Zn and P represented by core density functions in the extended wavefunction format. Non-covalent interaction calculations were performed with NCIPLOT[62] using pro-molecular electron densities and visualized with VMD.[63] Natural orbitals for chemical valence (NOCV)[64] analyses of **2** and **4** were performed with ADF2019.3[65] and were based on the interaction of the $[Ru(CO)_3(PPh_2C_6H_4)]^{2-}$ and $[Ru(IMe_4)_2(PPh_2C_6H_4)]^{2-}$ dianions with a Zn^{2+} center. Natural bond orbital analyses in the Supporting Information employed the NBO 6.0 program[66] with orbital plots displayed with Chemcraft.[67]

Results

Synthesis, structure and reactivity of Ru(ZnPhos)(CO)$_3$ (2). The serendipitous formation of ZnPhos complex **2** was observed initially following efforts to prepare a neutral analogue of the cationic $RuZn_2$ species, $[Ru(PPh_3)_2(C_6H_4PPh_2)(ZnMe)_2]^+$, reported recently as the product of reaction between $Ru(PPh_3)(C_6H_4PPh_2)_2(ZnMe)H$ and in-situ generated $[ZnMe]^+$.[41] Replacing $[ZnMe]^+$ by $ZnMe_2$ gave $Ru(PPh_3)(C_6H_4PPh_2)_2(ZnMe)_2$ (**1**; see Supporting Information for X-ray structure), which upon mild heating with CO resulted in the templated assembly of the ZnPhos ligand in **2** upon loss of PPh_3, formal elimination of $ZnMe_2$, insertion of the Ru-bound Zn atom between the two (ortho-diphenylphosphino)phenyl moieties and coordination of three CO ligands (Scheme 2). Given

that the central theme of the manuscript is the chemistry of Ru-ZnPhos complexes, a complete analysis of the bonding in **1** in comparison to $[Ru(PPh_3)_2(C_6H_4PPh_2)(ZnMe)_2]^+$ will be reported elsewhere.[68]

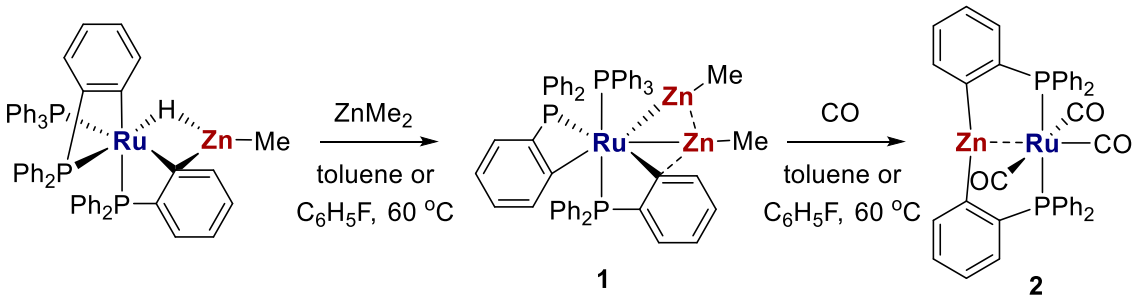

Scheme 2 Synthesis of the $RuZn_2$ complex **1** and reaction with CO to give **2**

A one-pot route to **2** was subsequently devised, which entailed sequential treatment of $Ru(PPh_3)_3HCl$ with $LiCH_2TMS$, $ZnMe_2$ and CO (Scheme 3). Not only did this afford **2** in good isolated yields (ca. 65%), but it could be carried out within one day, rather than ca. 1.5 weeks starting from $Ru(PPh_3)(C_6H_4PPh_2)_2(ZnMe)H$, isolating clean **1** etc.

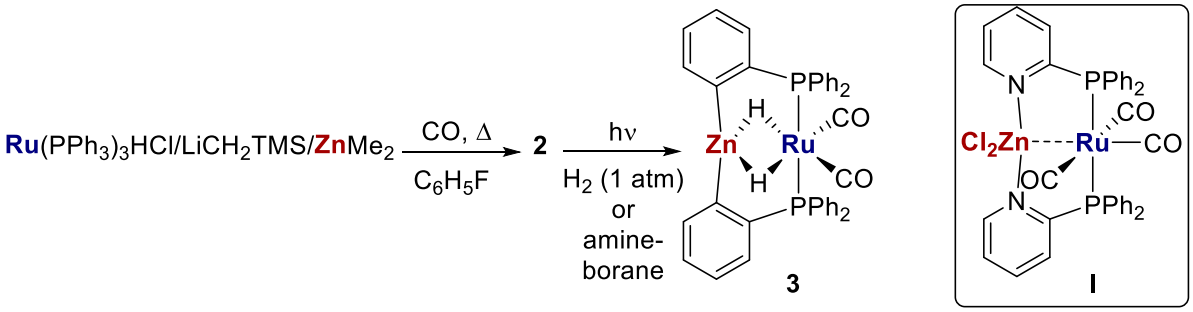

Scheme 3 Synthetic routes to **2** and subsequent reaction with H_2

Complex **2** was a yellow microcrystalline solid, which dissolved in both benzene and THF with mild warming. The X-ray crystal structure (Figure 1) confirmed the product as being a new member of the $Ru(P\text{-}P)(CO)_3$ (P-P = chelating phosphine) family.[69-72] The distorted trans axial arrangement of the phosphorus atoms (P-Ru-P = 159.35(2)°), along with

the mer-like orientation of the three CO ligands (e.g. C2-Ru-C3 = 152.01(11)°) gave a geometry markedly different from that in distorted square pyramidal Ru(Xantphos)$(CO)_3$[73] and one which is closer to that of Ru(2-$Ph_2PC_5H_4N)_2(CO)_3(ZnCl_2)$ (**I**, Scheme 3).[74,75] The Ru-CO bond length Ru-C1 (trans to Zn) was elongated (1.951(3) Å) relative to both Ru-C2 (1.929(3) Å) and Ru-C3 (1.923(3) Å). The Ru-Zn distance of 2.6878(4) Å (vide infra) was comparable to the sum of the two covalent radii.[76] IR spectroscopy showed the presence of three ν_{CO} bands at 2012, 1959 and 1931 cm^{-1}, ca. 20-30 cm^{-1} lower in frequency than found in **I**.[73]

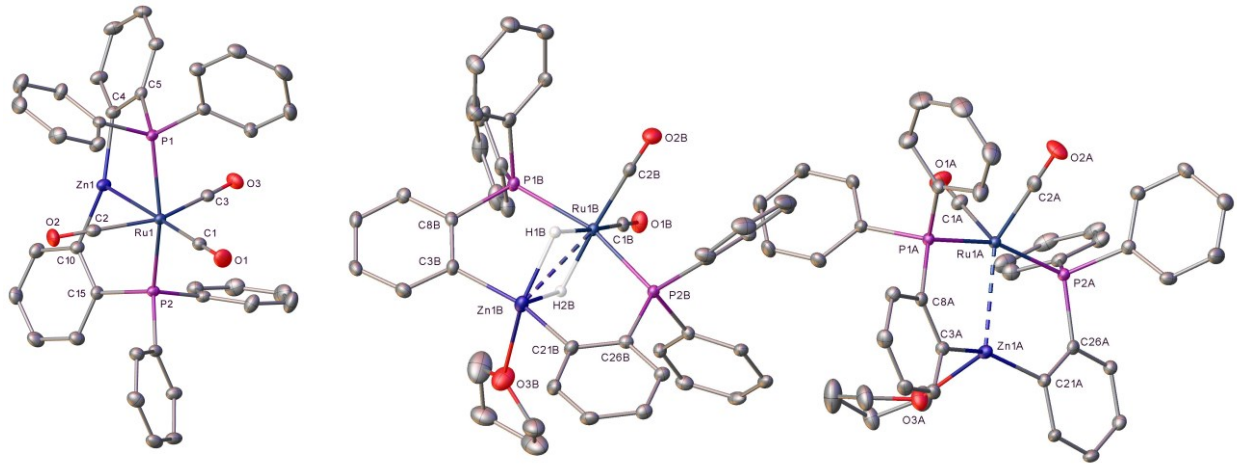

Figure 1. X-ray crystal structures of (left) **2** and **3** (middle and right). Thermal ellipsoids at 30%. All hydrogen atoms are removed for clarity, except for the hydrides, pertaining to the moiety based on Ru1B, that could be credibly refined in the structure of **3** (comparative hydride electron density in the molecule based on Ru1A did not converge sensibly). The minor, disordered, C40 component in **3** has also been omitted for clarity.

There was no evidence for loss of CO from **2** upon heating to 60 °C (under either argon or vacuum), or upon exposure to H_2 or PCy_3 at the same elevated temperature. However, UV photolysis of **2** in C_6D_6 or THF-d_8 under 1 atm H_2 resulted in loss of the ^{31}P

NMR resonance of the starting material (δ 61 in C_6D_6), and the appearance of a new product, Ru(ZnPhos)$(CO)_2(\mu\text{-}H)_2$ **3**, which exhibited a singlet ^{31}P resonance at δ 57 (in C_6D_6) and a triplet hydride resonance at δ -7.3 ($^2J_{HP}$ = 17.7 Hz). The molecular structure (Figure 1) afforded evidence for the generation of a dihydride complex resulting from H_2 addition across the Ru-Zn bond to form two bridging hydrides,[77-81] rather than by oxidative addition just to ruthenium.[82] Interestingly, there are two molecules in the asymmetric unit of **3** and the hydrides could be located credibly in one of these from the X-ray data. Despite a combination of twinning, a metal-dense core in the molecules present and the limitations of hydrogen location using X-rays, we were nonetheless able to record viable evidence for the hydrides in one of the molecules from the diffraction data. An overlay of the two molecules (Figure S20, Supporting Information) reveals the similarity of the Ru-Zn distances in both moieties. In terms of comparison, the structural metrics in **3** were largely unchanged from those in **2**, although the Ru-Zn distances in each of the two molecules within the asymmetric unit of **3** were lengthened (2.8080(9), 2.8184(9) Å), consistent with H_2 addition across the Ru-Zn bond.[77]

Formation of **3** was also possible through photochemical dehydrogenation of the amine boranes $H_3N{\cdot}BH_3$ or $Me_2HN{\cdot}BH_3$ by **2**.[83] The ^{11}B NMR spectrum confirmed that $[Me_2N\text{-}BH_2]_2$ was the major boron-containing product of the reaction with $Me_2HN{\cdot}BH_3$. With both H_2 and the amine boranes, prolonged photolysis led to the appearance of an additional hydride-containing product. Comparison of the hydride chemical shift (δ -6.34 in C_6D_6, δ -6.95 in THF-d_8) to literature data, as well as independent synthesis from $Ru(PPh_3)_2(CO)_3$, proved this was $Ru(PPh_3)_2(CO)_2H_2$.[43] It seems likely that cleavage of the Zn-$C_6H_4PPh_2$ bond[84,85] results from hydrolysis by adventitious moisture in the solvent or on the glassware. Indeed, there was a marked increase in the amount of $Ru(PPh_3)_2(CO)_2H_2$ formed when **2** was photolyzed under H_2 in degassed, but undried, C_6D_6 or THF-d_8.

Synthesis, structure and reactivity of Ru(ZnPhos)(IMe$_4$)$_2$ (4). Addition of an excess of the N-heterocyclic carbene IMe$_4$ (= 1,3,4,5-tetramethylimidazol-2-ylidene) to the mixture of Ru(PPh$_3$)$_3$HCl, LiCH$_2$TMS and ZnMe$_2$ (reaction from **1** was also possible) resulted again in formation of the ZnPhos ligand, but this time to afford the bis-IMe$_4$ complex Ru(ZnPhos)(IMe$_4$)$_2$ (**4**, Scheme 4). The product was obtained as dark-red blocks (UV-vis: 555, 460, 365 nm; vide infra) which were readily separable from the side product of the reaction, pale-yellow (IMe$_4$)$_2$ZnMe$_2$ (Figure S25).

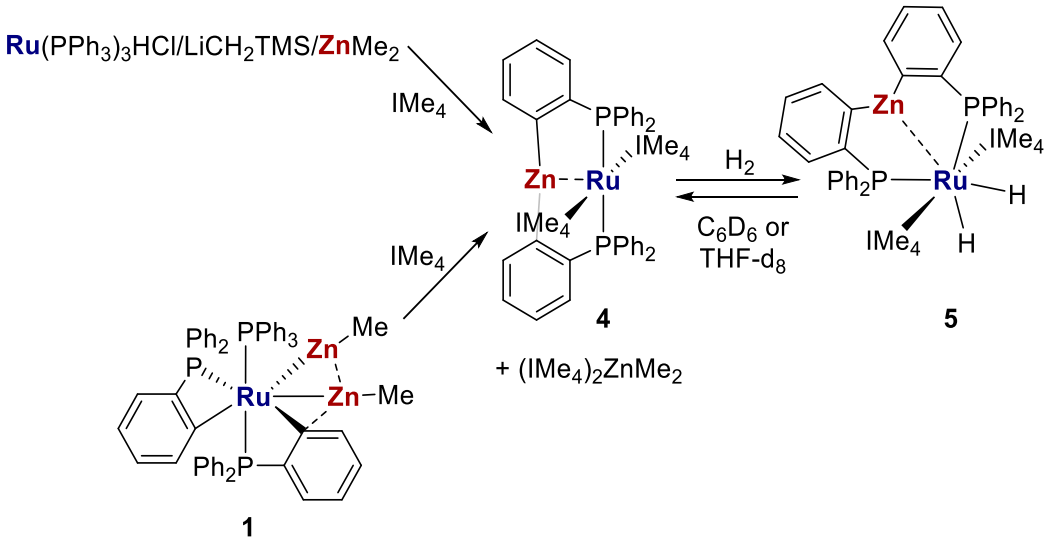

Scheme 4 Synthesis of **4** and reaction with H$_2$

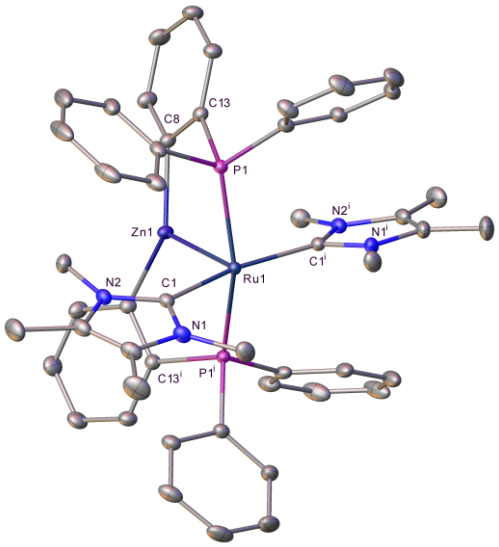

Figure 2. Molecular structure of **4**. Ellipsoids are represented at 30% probability and hydrogens have been omitted for clarity. [i] symmetry operation ½ – *x*, ³⁄₂ – *y*, *z*.

Complex **4** exhibited a distorted square pyramidal structure (Figure 2) with the ruthenium center bonded to zinc in the apical position and lying 0.085(1) Å below a basal plane comprising atoms P1, P1[i], C1 and C1[i]. The Ru-Zn bond length of 2.4958(3) Å is intermediate between the distance in **2** (2.6878(4) Å) and that in $[Ru(IPr)_2(CO)ZnEt]^+$ (2.4069(7) Å), which features a direct, unsupported Ru-Zn bond.[77]

NMR spectroscopic monitoring of the reaction of **4** with H_2 (1 atm) in THF showed immediate formation of the dihydride complex $Ru(ZnPhos)(IMe_4)_2H_2$ **(5**) in equilibrium with **4** (**4**:**5** ratio ca. 5:1). Increasing the temperature (60 °C) shifted the equilibrium further towards **4** (**4**:**5** ratio ca. 20:1), whereas upon cooling to low temperature (-60 °C), the solution changed color from dark red to pale red-orange, consistent with the increased concentration of **5** (**4**:**5** ratio ca. 1:4). Although the incomplete conversion precluded the possibility of isolating **5** for structural characterization, unequivocal evidence for the structure shown in Scheme 4 was provided by NMR spectroscopy, in particular, the AA′XX′ pattern of the Ru-H resonance at δ -6.57, which is consistent with the two hydride ligands both being trans to phosphorus.[86] The presence of a singlet in the $^{31}P\{^1H\}$ NMR spectrum confirmed that the termini of the ZnPhos ligand were equivalent, while both the appearance (triplet) and magnitude (9 Hz) of the splitting on the high frequency (δ 191) Ru-C_{NHC} signal in the $^{13}C\{^1H\}$ NMR spectrum was entirely consistent with the two IMe_4 ligands sitting cis to ZnPhos. This structure was also supported by DFT calculations that indicated a pentagonal bipyramidal structure (vide infra).

Computational Studies. The Ru-Zn interactions in **2** and **4** were investigated by a combination of quantum theory of atoms in molecules (QTAIM), non-covalent interaction

(NCI) plots and natural orbitals for chemical valence (NOCV) techniques (Figure 3). For both molecules QTAIM identifies a Ru-Zn bond path with BCP electron densities, ρ(r), of 0.042 au and 0.056 au for **2** and **4** respectively. The Ru-Zn BCPs also exhibit ellipticities, ε, below 0.1, indicative of σ-interactions as well as small, negative total energy densities, H(r), suggesting a degree of covalent character. For comparison, the Ru-P BCPs in **2** and **4** exhibit a similar pattern, albeit with larger values of ρ(r) and H(r). The P→Ru dative interactions are thus stronger than the Ru-Zn interactions, but the latter are significant in both **2** and **4**, and somewhat stronger in **4**. The direct Ru→Zn interaction in $[Ru(IPr)_2(CO)ZnEt]^+$ has a higher ρ(r) of 0.071 au, reflecting the shorter Ru-Zn distance of 2.4069(7) Å in that case.[87, 88]

The presence of significant Ru-Zn interactions in **2** and **4** was confirmed by the NCI and NOCV analyses. NCI plots for **2** and **4** both exhibit a turquoise region along the Ru-Zn vector that indicates a stabilization, but for **4** the more intense and localized nature of this feature reflects a stronger interaction. NOCV analyses identified one major deformation density channel in each system that corresponds to electron donation from Ru to Zn. This is stronger in **4** (ΔE_{orb} = 87.1 kcal/mol) with a charge flow of 0.6 e, approximately twice that computed for **2**. Overall, the various analyses indicate a significant Ru→Zn Z-type donation in both **2** and **4**, with this being significantly stronger in **4**.[89] Although **4** features a 16e Ru center, this is clearly more electron rich than the 18e Ru center in **2**, reflecting the presence of two strongly electron-donating IMe_4 ligands in this species rather than three electron-withdrawing carbonyls in **2**.

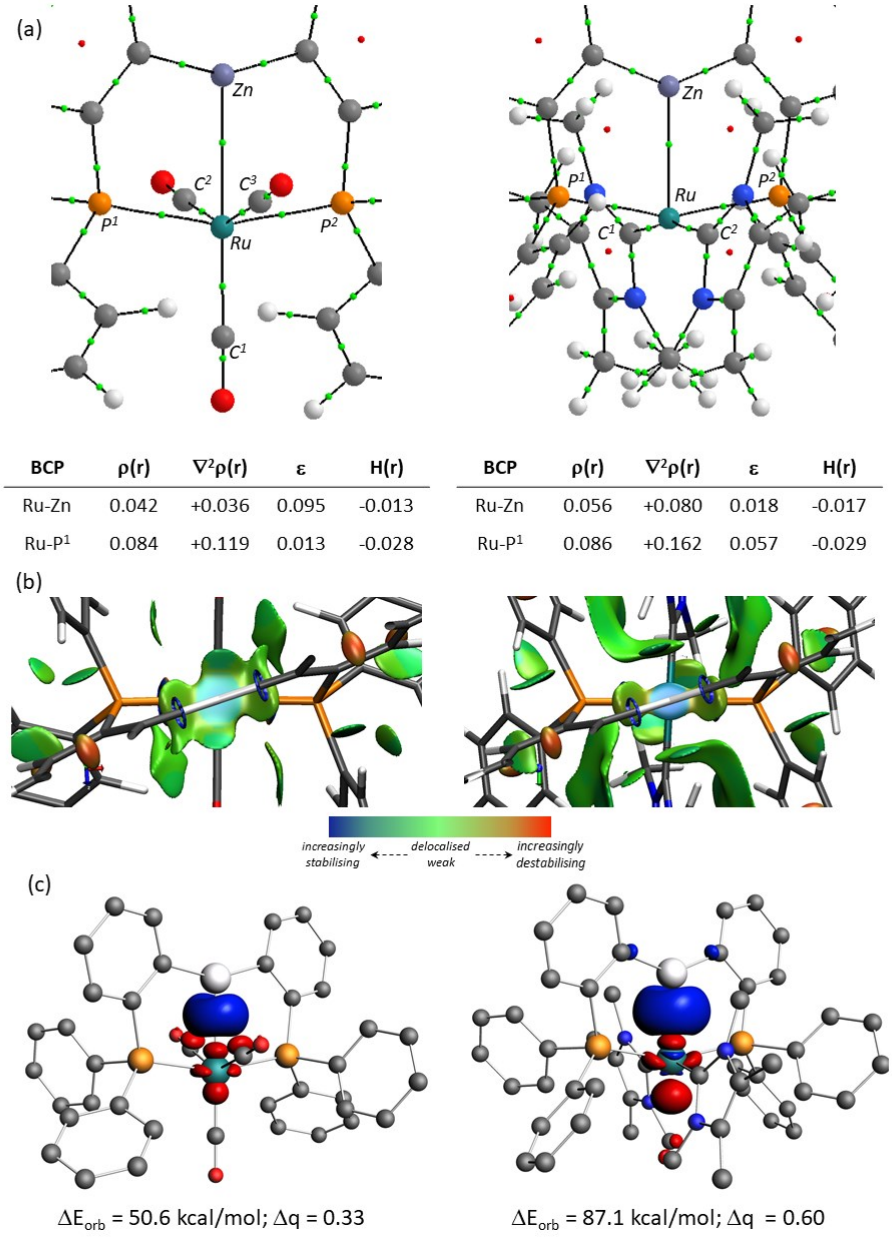

BCP	ρ(r)	∇²ρ(r)	ε	H(r)
Ru-Zn	0.042	+0.036	0.095	-0.013
Ru-P¹	0.084	+0.119	0.013	-0.028

BCP	ρ(r)	∇²ρ(r)	ε	H(r)
Ru-Zn	0.056	+0.080	0.018	-0.017
Ru-P¹	0.086	+0.162	0.057	-0.029

Figure 3. Electronic structure analyses of **2** (left) and **4** (right). (a) Details of the QTAIM molecular graphs with BCPs and RCPs shown as green and red spheres respectively and selected BCP metrics shown in atomic units. (b) NCI plots looking down the Zn-Ru vector; isosurfaces generated for s = 0.3 au and $-0.07 < \rho < 0.07$ au. (c) NOCV contour plots (isovalue 0.003 au) of the key deformation density channel describing Ru→Zn donation in **2** and **4**. Calculations were based on interaction of the $[Ru(CO)_3(PPh_2C_6H_4)]^{2-}$ and

$[Ru(IMe_4)_2(PPh_2C_6H_4)]^{2-}$ dianions with a Zn^{2+} center. Electron flow is shown from red to blue and H atoms are omitted for clarity.

The different reactivities of **2** and **4** with H_2 were also modeled with DFT calculations. Photolysis of **2** forms Ru(ZnPhos)$(CO)_2$ (**2-CO**) for which a series of square-pyramidal isomers is computed with Zn occupying one coordination site (Figure 4(a)). The most stable isomer, ***mer,cis*-2-CO** (i.e. with a *mer*-PZnP arrangement and *cis*-CO ligands), is formed via loss of CO_{cis} and lies 23.7 kcal/mol above **2**. ***mer,trans*-2-CO_1**, formed upon loss of CO_{trans} in **2** is 2.2 kcal/mol above ***mer,cis*-2-CO** and the two can readily interconvert via ***mer,trans*-2-CO_2**. ***mer,trans*-2-CO_2** and ***mer,trans*-2-CO_1** differ primarily in their Zn-Ru-C angles (ca. 77° and 107° respectively). ***fac,cis*-2-CO_P** (+6.0 kcal/mol) and ***fac,cis*-2-CO_{Zn}** (+3.7 kcal/mol, where the subscripted atom indicates the axial ligand of the square-pyramid) are also accessible via a barrier of 13.0 kcal/mol.

Figure 4(b) compares the computed structures of ***mer,trans*-2-CO_1**, ***mer,cis*-2-CO** and ***fac,cis*-2-CO_{Zn}** and highlights the ability of the ZnPhos ligand to access both κ^3-mer- and fac-P,Zn,P binding modes. This has parallels to the geometrically related DPEphos ligand[90] but now with a central Lewis acidic binding site. Computed Ru-Zn distances in these species are all within the range of 2.62-2.73 Å[91] and so not markedly different to the Ru-Zn distance of 2.6878(4) Å in **2**. The cisoid {$RuP_2(CO)_2$} moieties in ***mer,trans*-2-CO_1** and ***mer,cis*-2-CO** are similar to that seen in Ru($P^tBu_2Me)_2(CO)_2$ ($\angle$CRuC = 133.3(4)°, $\angle$PRuP = 165.56(8)°)[92, 93] and a distinct bending of the Ru-CO units (cf. $\angle$RuCO ≈ 165°) is also noticeable. These distortions are characteristic of strong back-donation from a highly electron-rich Ru(0) center and imply a similar degree of electron rich Ru(0) character is retained in these isomers of **2-CO**.

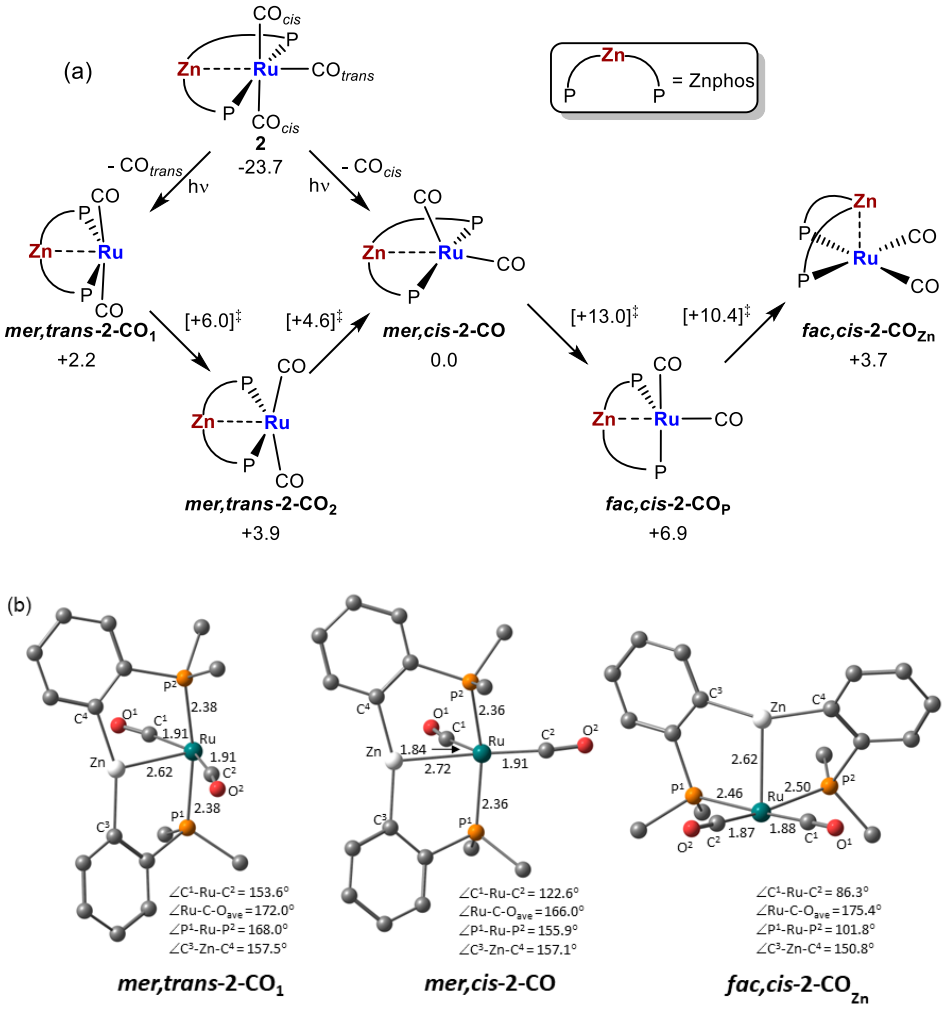

Figure 4. (a) Computed isomers of Ru(ZnPhos)(CO)$_2$ (**2-CO**) with free energies in kcal/mol and isomerization transition state energies shown in square brackets and (b) computed geometries of ***mer,trans*-2-CO$_1$**, ***mer,cis*-2-CO** and ***fac,cis*-2-CO$_{Zn}$** with selected distances (Å) and angles (°). Ph substituents are truncated at the ipso carbon and hydrogen atoms are omitted for clarity.

For Ru(ZnPhos)(IMe$_4$)$_2$ (**4**) three isomers were computed of which the species observed experimentally (***mer,trans*-4**) is clearly the most stable (Figure 5). ***mer,cis*-4** and ***fac,cis*-4** are 24.3 kcal/mol and 12.0 kcal/mol higher in energy and interconversion from ***mer,trans*-4** entails a barrier of 30.7 kcal/mol. This is in strong contrast to the CO analogues

where all isomers of **2-CO** are kinetically accessible, and this difference ultimately has a significant bearing on the reactivity of the two systems (vide infra).

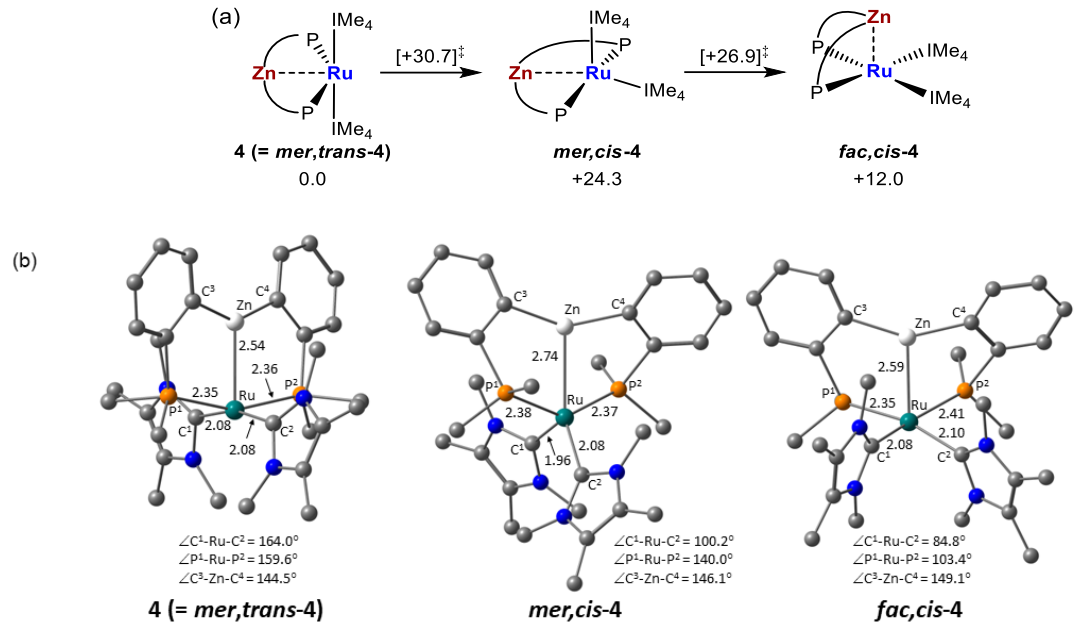

Figure 5. (a) Computed isomers of Ru(ZnPhos)(IMe_4)$_2$ (**4**) with free energies in kcal/mol and isomerization transition state energies shown in square brackets and (b) computed geometries of ***mer,trans*-4**, ***mer,cis*-4** and ***fac,cis*-4** with selected distances (Å) and angles (°). Ph substituents are truncated at the ipso carbon and hydrogen atoms are omitted for clarity.

Computed pathways for H_2 activation were assessed for all isomers of both **2-CO** and **4** and the most relevant pathways are compared in Figures 6(a) and 6(b), respectively, with selected computed structures shown in Figure 6(c). Details of alternative pathways are provided in Figures S34 and S35. Activation of H_2 at ***mer,cis*-2-CO** proceeds in a single step via **TS(2-3)1**$_{mer,cis}$ at +6.7 kcal/mol. **TS(2-3)1**$_{mer,cis}$ corresponds to H_2 adding to the Ru center but leads directly to cleavage of the H-H bond to give **Int(2-3)**$_{mer,cis}$ with one terminal and one bridging hydride. Movement of the bridging hydride across the Ru···Zn vector via **TS(2-3)2**$_{mer,cis}$ at -4.2 kcal/mol induces the terminal hydride to move into the second bridging

position to give **3** at -20.2 kcal/mol. The structure of **TS(2-3)2**$_{mer,cis}$ reiterates the flexibility of the ZnPhos ligand with the P-Ru-P angle narrowing to 148º, the Ru···Zn distance increasing to over 3.3 Å and the C^3-Zn-C^4 angle widening to 174° to accommodate the near-linear Zn-H^1-Ru moiety.

In principle, **3** could also be formed via reaction of H_2 with ***mer,trans*-2-CO**$_1$ and the initial oxidative addition occurs with a barrier of only +3.5 kcal/mol to form cis-dihydride intermediate **Int(2-3)1**$_{mer,trans}$ at -5.9 kcal/mol. The onward pathway involves isomerization to a trans-dihydride isomer, **Int(2-3)2**$_{mer,trans}$, in which one hydride bridges Ru and Zn. This step, however, proceeds with a relatively high barrier of 23.3 kcal/mol via a trigonal prismatic transition state, **TS(2-3)2**$_{mer,trans}$. A more accessible route to **3** from **Int(2-3)1**$_{mer,trans}$ is via reductive elimination of H_2 and isomerization to form ***mer,cis*-2-CO** which can then react with H_2 as described above. This process has an overall barrier (relative to **Int(2-3)1**$_{mer,trans}$) of only 12.6 kcal/mol. Thus the formation of **3**, either through the direct reaction of H_2 with ***mer,cis*-2-CO** or through the reversible formation of **Int(2-3)1**$_{mer,trans}$, occurs with low barriers and, relative to these species, is strongly thermodynamically favored, all consistent with the efficient formation of **3** seen experimentally.[94]

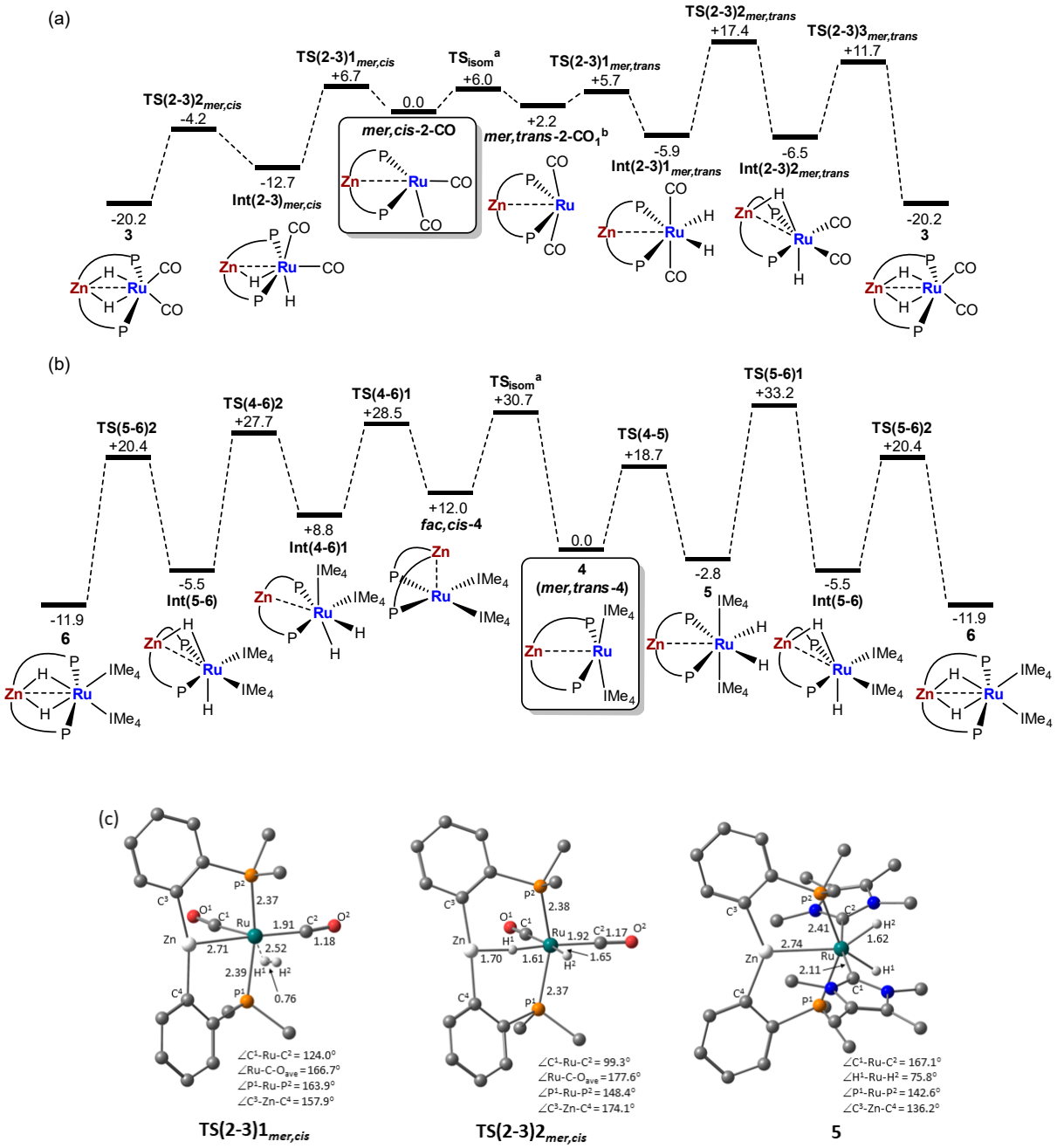

Figure 6. Computed reaction profiles (free energies, kcal/mol) for the reactions of (a) ***mer,cis*-2-CO** with H_2 and (b) **4** with H_2. (c) Computed geometries of key stationary with selected distances (Å) and angles (°). Ph substituents are truncated at the ipso carbon and non-reacting hydrogen atoms are omitted for clarity. [a]only the energy of the highest lying transition state involved in the isomerisations of **2-CO** and **4** are indicated as **TS_{isom}** – see Figures 4 and 5 for details. [b]H_2 oxidative addition at ***mer,trans*-2-CO_1** involves several steps

and the energy of the highest-lying transition state (corresponding to the H_2 addition step) is indicated. See Figure S34 for full details.

The related reactions of **4** are summarized in Figure 7(b). Oxidative addition of H_2 at **4** proceeds with an accessible barrier of 18.7 kcal/mol to give the cis-dihydride **5** at -2.8 kcal/mol. The formation of **6** (the IMe_4 analogue of **3**) is computed to be thermodynamically feasible (ΔG = -11.9 kcal/mol). However, the isomerization of **5** to the trans dihydride intermediate **Int(5-6)** is kinetically inaccessible with a computed barrier of 36.0 kcal/mol. Moreover, reactions via ***mer,cis*-4** or ***fac,cis*-4** are both kinetically blocked by the prohibitively high barrier to isomerization (30.7 kcal/mol) and the subsequent high energy transition states for H_2 oxidative addition: +28.5 kcal/mol for ***fac,cis*-4** (i.e. via **TS(4-6)1**, Figure 6(b)) and +40.1 kcal/mol for ***mer,cis*-4** (Figure S36). Therefore, only the equilibrium between **4** and H_2 to form **5** is accessible, and the small computed thermodynamic preference for **5** is qualitatively consistent with this species being preferentially formed at low temperature.

The computed structure of **5** (Figure 6(c)) displays effective C_2 symmetry and resembles a pentagonal bipyramid with Zn lying in the equatorial plane along with the hydride and phosphorus centers. The computed Ru-Zn distance of 2.74 Å is 0.2 Å longer than in the computed structure of **4**, but QTAIM still identifies a Ru-Zn bond path with a BCP $\rho(r)$ of 0.041 au. While this is somewhat smaller than in **4** (0.056 au) it suggests a Ru→Zn interaction is retained in **5**, a view supported by NCI, NOCV and NBO calculations (see Figure S32).

Discussion

Experimentally **2** reacts upon photolysis with H_2 to form the bridged dihydride **3** whereas **4** forms the terminal dihydride **5**. The calculations link these different outcomes to the accessibility of ***mer,cis*-2-CO** (and its facile interconversion with ***mer,trans*-2-CO$_1$**), whereas the IMe_4 analogue, ***mer,cis*-4** lies +24.3 kcal/mol above ***fac,cis*-4** and is therefore inaccessible. These differences can be rationalized in terms of the behavior of the two different 16e Ru(0) $\{RuP_2L_2\}$ fragments contained within these Ru(ZnPhos)L_2 systems.

Figure 4(b) shows the computed structures of ***mer,cis*-2-CO** and ***mer,trans*-2-CO$_1$** to be related by rotation of the $\{Ru(CO)_2\}$ moiety around the pseudo P-Ru-P axis. Major changes to the core $\{RuZnP_2(CO)_2\}$ geometry are in the CRuC angle (***mer,cis*-2-CO**: 122.6°; ***mer,trans*-2-CO$_1$**: 153.6°) with a smaller widening of the PRuP angle (by 12.1°) and shortening of the Ru-Zn distance (by 0.1 Å). To highlight the effect of changing the CRuC angle, calculations were performed on a simple *trans*-$Ru(PH_3)_2(CO)_2$ model system in which this angle was varied from 120º to 160°. Computed energies (Figure S37) show a variation of less than 2 kcal/mol across this range, indicating that the $\{RuP_2(CO)_2\}$ fragment within **2-CO** can readily accommodate the geometric changes required for the interconversion between ***mer,cis*-2-CO** and ***mer,trans*-2-CO$_1$**. This in turn reflects the ability of CO to act as a potent π-acceptor within the distorted C_{2v} $\{RuP_2(CO)_2\}$ fragment.[92,93]

In contrast, the core $\{RuZnP_2C_2\}$ fragment within the equivalent isomers of **4** undergoes far more distortion, with the CRuC and PRuP angles narrowing by ca. 64° and 20° respectively from ***mer,trans*-4** to and the Ru-Zn distance elongating by 0.2 Å (Figure 5(b)). We did consider the possibility that the proximity of the bulky PPh_2 and IMe_4 groups rendered the more compact geometry of ***mer,cis*-4** less accessible for steric reasons. To probe this we computed ΔE, the difference in energy between these two isomers, for a model system, $Ru(ZnPhos^H)(IH_4)_2$ ($ZnPhos^H$ = $Zn(o\text{-}C_6H_4PH_2)_2$, IH = 1,3-dihydroimidazol-2-ylidene), in which the $\{RuZnP_2C_2\}$ atoms were fixed at the positions optimized for the full

system (Figure 7, Entry 2). However, comparison with the full system (Entry 1) showed ΔE actually increases from +22.8 kcal/mol to +24.4 kcal/mol, thus ruling out any steric effect. The destabilization of ***mer,cis*-4** must therefore arise from the distortion of the d^8 {RuP_2C_2} fragment and this was probed using a *trans*-$Ru(PH_3)_2(IH)_2$ model system. In this case changing the CRuC angle from 164° to 100° (the values in ***mer,trans*-4** and ***mer,cis*-4**) increased the energy by more than 18 kcal/mol (Figure S37). This reflects the strong destabilization of an occupied d-orbital upon narrowing the CRuC angle[95] without the possibility of the significant stabilization through π-back donation to the IMe_4 ligands.[96]

To assess the role of the Zn center in the ***mer,trans*-4** and ***mer,cis*-4** isomerization, the Zn-free $Ru(PPh_3)_2(IMe_4)_2$ system was computed, again with a fixed {RuP_2C_2} geometry (Figure 7, Entry 3). Comparison with Entry 1 shows ΔE reduces by 4.9 kcal/mol to +17.9 kcal/mol. This implies that any stabilization due to the Ru→Zn interaction in ***mer,trans*-4** is significantly reduced in ***mer,cis*-4** and is consistent with the significantly longer Ru-Zn distance in the latter.

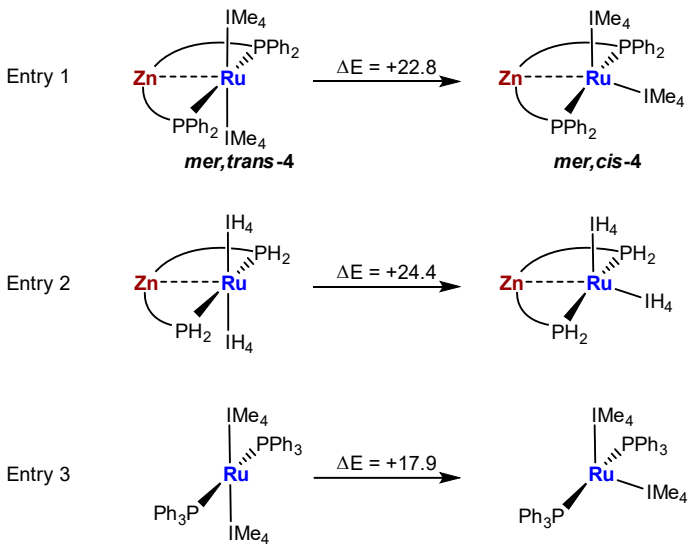

Figure 7. Computed values for ΔE (kcal/mol), the difference in energy for ***mer,trans*-4** and ***mer,cis*-4** computed with different model systems. For Entries 2 and 3 the {$RuZnP_2C_2$} and {RuP_2C_2} cores were fixed at the positions computed for ***mer,trans*-4** and ***mer,cis*-4**. The geometries in Entries 2 and 3 do not correspond to true minima and so all energies are based on electronic (SCF) energies.

The above analyses suggest that these Ru(ZnPhos)L_2 species can be considered as 4-coordinate 16e Ru(0)L_4 species that are stabilized by interaction with a Lewis acidic Zn center. This is supported by the red color of species **4**, absorption in the visible region of the electronic spectrum also being a feature of other 16e Ru(0)L_4 complexes.[92,93,97-99] Indeed, the three-band electronic spectrum of **4** with peaks at 555, 460, and 365 nm[100] resembles that of Ru(dmpe)$_2$ (dmpe=1,2-bis(dimethylphosphino)ethane), albeit with a distinct blue-shift.[101] To date examples of stable 16e Ru(0)L_4 species have featured strong π-acceptor CO/NO ligands;[92,93,97-99,102] in contrast Ru(dmpe)$_2$ is a transient species only observed in low temperature noble gas matrices or upon flash photolysis. Thus, the room temperature preparation and characterization of Ru(ZnPhos)(IMe_4)$_2$, a system devoid of strong π-acceptors, is remarkable and highlights the role of the Lewis acidic Zn in stabilizing the Ru(0) center in this system. This also suggests the possibility of using heterobimetallic TM→MG Z-type interactions to stabilize novel low valent transition metal centers.[25]

Conclusions

This paper details the preparation and characterization of Ru(ZnPhos)$(CO)_3$ (**2**) and Ru(ZnPhos)(IMe_4)$_2$ (**4**) where ZnPhos is the novel Zn(o-$C_6H_4PPh_2$)$_2$ chelating ligand. ZnPhos, a structural analogue of DPEphos that features a central Group 12 Z-type acceptor binding site, assembled within **2** and **4** via the in-situ reactions of

$Ru(PPh_3)(C_6H_4PPh_2)_2(ZnMe)_2$ or $Ru(PPh_3)_3HCl/LiCH_2TMS/ZnMe_2$ with CO or IMe_4. Computational analysis shows the presence of direct Ru→Zn interactions in both 18e **2** and 16e **4**, with this being somewhat stronger in the latter. This reflects the greater donor capacity of the IMe_4 ligands compared to CO that results in a stronger Ru-Zn interaction in **4** despite its lower formal electron count at Ru.

The reactions of **2** (under photolytic conditions) and **4** with H_2 gave distinct outcomes. For **2**, photolytic dissociation of CO in presence of H_2 leads to $Ru(ZnPhos)(CO)_2(\mu\text{-}H)_2$ (**3**) in which H_2 adds across the Ru-Zn bond and both hydrides lie cis to the phosphines. In contrast **4** adds H_2 directly at room temperature to give an equilibrium mixture with $Ru(ZnPhos)(IMe_4)_2H_2$ (**5**) featuring terminal hydrides at Ru. **5** is characterized spectroscopically as having hydrides trans to the phosphines, and calculations indicate a trigonal pentagonal geometry with axial IMe_4 ligands and a Ru→Zn interaction in the equatorial plane. DFT calculations rationalize the different reactivities of **2** and **4** with H_2 in terms of the much greater ease of distorting the 16e $Ru(ZnPhos)(CO)_2$ intermediate formed upon photolysis compared to its isoelectronic $Ru(ZnPhos)(IMe_4)_2$ congener. This in turn reflects the much stronger π-acceptor ability of CO over a strongly e-donating NHC such as IMe_4. Calculations also highlight the range of structures accessible to the ZnPhos ligand, including mer- and fac-PZnP binding modes and flexible Ru-Zn distances spanning 2.5 Å to 3.3 Å.

Complex **4** can be considered as comprising a Zn-stabilized 16e $Ru(0)L_4$ center and as such this species displays remarkable stability under anhydrous conditions at room temperature. All previous examples of crystallographically characterized 16e $Ru(0)L_4$ species have featured strong π-accepting CO or NO ligands. The presence of the Ru→Zn interaction is therefore be crucial in stabilizing a $Ru(0)L_4$ species that is devoid of strong π-acceptor ligands. Further studies will seek to extend the synthesis of ZnPhos to other Element-Phos

ligands that have to date proved inaccessible, and to explore the use of such ligands to stabilize other novel low-valent transition metal centers along with their ability towards small molecule activation and catalysis.

Conflicts of Interest There are no conflicts of interest to report.

Acknowledgements This project has received funding from the European Union's Horizon 2020 research and innovation programme under the Marie Skłodowska-Curie grant agreement No 792674 (FMM). We also acknowledge financial support from the EPSRC in the form of DTP studentships to CJI and ALB. We dedicate this paper to Professor Alan Welch on the occasion of his retirement from Heriot-Watt University.

Associated Content

Supporting Information The supporting information is available free of charge at……. Experimental and computational details. Spectra of **1**-**5**. Molecular structures of $Ru(PPh_3)(C_6H_4PPh_2)_2(ZnMe)_2$ and $(IMe_4)_2ZnMe_2$. CCDC 1995946-1995948, 2003689 and 2031254 (PDF).

References

(1) Green, M. L. H.; Parkin, G. Application of the covalent bond classification method for the teaching of inorganic chemistry. *J. Chem. Ed.* **2014**, *91*, 807-816.

(2) Amgoune, A.; Bourissou, D. σ-Acceptor, Z-type ligands for transition metals. *Chem. Commun.* **2011**, *47*, 859-871.

(3) Bouhadir, G.; Bourissou, D. Coordination of Lewis acids to transition metals: Z-type ligands. *Struct. Bond.* **2017**, *171*, 141-201.

(4) You, D.; Gabbaï, F. P. Tunable σ-accepting Z-type ligands for organometallic catalysis. *Trends in Chemistry* **2019**, *1*, 485-496.

(5) Sircoglou, M.; Bontemps, S.; Bouhadir, G.; Saffon, N.; Miqueu, K.; Gu, W.; Mercy, M.; Chen, C.-H.; Foxman, B. M.; Maron, L.; Ozerov, O. V.; Bourissou, D. Group 10 and 11 metal boratranes (Ni, Pd, Pt, CuCl, AgCl, AuCl, and Au^{+}) derived from a triphosphine-borane. *J. Am. Chem. Soc.* **2008**, *130*, 16729-16738.

(6) Bontemps, S.; Bouhadir, G.; Gu, W.; Mercy, M.; Chen, C.-H.; Foxman, B. M.; Maron, L.; Ozerov, O. V.; Bourissou, D. Metallaboratranes derived from a triphosphanyl-borane: Intrinsic C_3 symmetry supported by a Z-type ligand. *Angew. Chem. Int. Ed.* **2008**, *47*, 1481-1484.

(7) Derrah, E. J.; Sircoglou, M.; Mercy, M.; Ladeira, S.; Bouhadir, G.; Miqueu, K.; Maron, L.; Bourissou, D. Original transition metal→indium interactions upon coordination of a triphosphine-indane. *Organometallics* **2011**, *30*, 657-660.

(8) Moret, M.-E.; Peters, J. C. Terminal iron dinitrogen and iron imide complexes supported by a tris(phosphino)borane ligand. *Angew. Chem. Int. Ed.* **2011**, *50*, 2063-2067.

(9) Lin, T.-P.; Gabbaï, F. P. Two-electron redox chemistry at the dinuclear core of a TePt platform: Chlorine photoreductive elimination and isolation of a $Te^{V}Pt^{I}$ complex. *J. Am. Chem. Soc.* **2012**, *134*, 12230-12238.

(10) Harman, W. H.; Peters, J. C. Reversible H_2 addition across a nickel-borane unit as a promising strategy for catalysis. *J. Am. Chem. Soc.* **2012**, *134*, 5080-5082.

(11) Kameo, H.; Nakazawa, H. Recent developments in the coordination chemistry of multidentate ligands featuring a boron moiety. *Chem. Asian. J.* **2013**, *8*, 1720-1734.

(12) MacMillan, S. N.; Harman, W. H.; Peters, J. C. Facile Si-H bond activation and hydrosilylation catalysis mediated by a nickel-borane complex. *Chem. Sci.* **2014**, *5*, 590-597.

(13) Suess, D. L. M.; Tsay, C.; Peters, J. C. Dihydrogen binding to isostructural $S = ½$ and $S = 0$ cobalt complexes. *J. Am. Chem. Soc.* **2012**, *134*, 14158-14164

(14) Sircoglou, M.; Saffon, N.; Miqueu, K.; Bouhadir, G.; Bourissou, D. Activation of M-Cl bonds with phosphine-alanes: Preparation and characterization of zwitterionic gold and copper complexes. *Organometallics* **2013,** *32*, 6780-6784.

(15) Suess, D. L. M.; Peters, J. C. H-H and Si-H bond addition to $Fe{\equiv}NNR_2$ intermediates derived from N_2. *J. Am. Chem. Soc.* **2013**, *135*, 4938-4941.

(16) Yang, H.; Gabbaï, F. P. Solution and solid-state photoreductive elimination of chlorine by irradiation of a $[PtSb]^{VII}$ complex. *J. Am. Chem. Soc.* **2014**, *136*, 10866-10869.

(17) Cowie, B. E.; Tsao, F. A.; Emslie, D. J. H. Synthesis and platinum complexes of an alane-appended 1,1'-bis(phosphino)ferrocene ligand. *Angew. Chem. Int. Ed.* **2015**, *54*, 2165-2169.

(18) Cammarota, R. C.; Lu, C. C. Tuning nickel with Lewis acidic group 13 metalloligands for catalytic olefin hydrogenation. *J. Am. Chem. Soc.* **2015**, *137*, 12486-12489.

(19) Bouhadir, G.; Bourissou, D. Complexes of ambiphilic ligands: Reactivity and catalytic applications. *Chem. Soc. Rev.* **2016**, *45*, 1065-1079.

(20) Jones, J. S.; Gabbaï, F. P. Coordination- and redox-noninnocent behavior of ambiphilic ligands containing antimony. *Acc. Chem. Res.* **2016**, *49*, 857-867.

(21) Cammarota, R. C.; Vollmer, M. V.; Xie, J.; Ye, J.; Linehan, J. C.; Burgess, S. A.; Appel, A. A.; Gagliardi, L.; Lu, C. C. A bimetallic nickel-gallium complex catalyzes CO_2 hydrogenation via the intermediacy of an anionic d^{10} nickel hydride *J. Am. Chem. Soc.* **2017**, *139*, 14244-14250.

(22) Cammarota, R. C.; Clouston, L. J.; Lu, C. C. Leveraging molecular metal-support interactions for H_2 and N_2 activation. *Coord. Chem. Rev.* **2017**, *334*, 100-111.

(23) Takaya, J.; Iwasawa, N. Synthesis, structure and catalysis of palladium complexes bearing a group 13 metalloligand: Remarkable effect of an aluminium-metalloligand in hydrosilylation of CO_2. *J. Am. Chem. Soc.* **2017**, *139*, 6074-6077.

(24) Jones, J. S.; Gabbaï, F. P. Activation of an Au-Cl bond by a pendent Sb^{III} Lewis acid: Impact on structure and catalytic activity. *Chem. Eur. J.* **2017**, *23*, 1136-1144.

(25) Vollmer, M. V.; Ye, J.; Linehan, J. C.; Graziano, B. J.; Preston, A.; Wiedner, E. S.; Lu, C. C. Cobalt-group 13 complexes catalyze CO_2 hydrogenation via a Co(-I)/Co(I) redox cycle. *ACS Catal.* **2020**, *10*, 2459-2470.

(26) Bennett, M. A.; Bhargava, S. K.; Mirzadeh, N.; Privér, S. H. The use of $[2\text{-}C_6R_4PPh_2]^-$ (R = H, F) and related carbanions as building blocks in coordination chemistry. *Coord. Chem. Rev.* **2018**, *370*, 69-128.

(27) Lin, T.-P.; Ke, I.-S.; Gabbaï, F. P. σ-Accepting properties of a chlorobismuthine ligand. *Angew. Chem. Int. Ed.* **2012**, *51*, 4985-4988.

(28) Sircoglou, M.; Bontemps, S.; Mercy, M.; Saffon, N.; Takahashi, M.; Bouhadir, G.; Maron, L.; Bourissou, D. Transition-metal complexes featuring Z-type ligands: Agreement or discrepancy between geometry and dn configuration? *Angew. Chem. Int. Ed.* **2007**, *46*, 8583-8586.

(29) Kameo, H.; Nakazawa, H. Synthesis of a rhodium complex featuring the Rh-H-B linkage via a hydride migration from rhodium to borane: Study on the electronic deviation induced by the presence of the boron moiety. *Organometallics* **2012**, *31*, 7476-7484.

(30) Harman, W. H.; Lin, T.-P.; Peters, J. C. A d^{10} Ni-(H_2) adduct as an intermediate in H-H oxidative addition across a Ni-B bond. *Angew. Chem. Int. Ed.* **2014**, *53*, 1081-1086.

(31) Shih, W.-C.; Gu, W.; MacInnes, M. C.; Timpa, S. D.; Bhuvanesh, N.; Zhou, J.; Ozerov, O. V. Facile insertion of Rh and Ir into a boron-phenyl bond leading to

boryl/bis(phosphine) PBP pincer complexes. *J. Am. Chem. Soc.* **2016**, *138*, 2086-2089.

(32) Kameo, H.; Yamamoto, J.; Asada, A.; Nakazawa, H.; Matsuzaka, H.; Bourissou, D. Palladium-borane cooperation: Evidence for an anionic pathway and its application to catalytic hydro-/deutero-dechlorination. *Angew. Chem. Int. Ed.* **2019**, *58*, 18783-18787.

(33) Tschersich, C.; Limberg, C.; Roggan, S.; Herwig, C.; Ernsting, N.; Kovalenko, S.; Mebs, S. Gold- and platinum-bismuth donor-acceptor interactions supported by an ambiphilic PBiP pincer ligand. *Angew. Chem. Int. Ed.* **2012**, *51*, 4989-4992.

(34) Tschersich, C.; Hoof, S.; Frank, N.; Herwig, C.; Limberg, C. The effect of substituents at Lewis acidic bismuth(III) centres on its propensity to bind a noble metal donor. *Inorg. Chem.* **2016**, *55*, 1837-1842.

(35) You, D.; Yang, H.; Sen, S.; Gabbaï, F. P. Modulating the σ-accepting properties of an antimony Z-type ligand via anion abstraction: Remote-controlled reactivity of the coordinated platinium atom. *J. Am. Chem. Soc.* **2018**, *140*, 9644-9651.

(36) Bennett, M. A.; Contel, M.; Hockless, D. C. R.; Welling, L. T. Bis{(2-diphenylphosphino)phenyl}mercury: A novel bidentate ligand and transfer reagent for the o-$C_6H_4PPh_2$ group. *Chem. Commun.* **1998**, 2401-2402.

(37) Bennett, M. A.; Contel, M.; Hockless, D. C. R.; Welling, L. T.; Willis, A. C. Bis{(2-diphenylphosphino)phenyl}mercury: A P-donor ligand and precursor to mixed metal-mercury (d_8-d^{10}) cyclometalated complexes containing 2-$C_6H_4PPh_2$. *Inorg. Chem.* **2002**, *41*, 844-855.

(38) López-de-Luzuriaga, J. M.; Monge, M.; Olmos, M. E.;Pascual, D. Study of the nature of closed shell $Hg^{II}\cdots M^{I}$ (M = Cu, Ag, Au) interactions. *Organometallics* **2015**, *34*, 3029-3038.

(39) For a more general consideration of TM-Zn interactions, see: (a) Bollermann, T.; Gemel, C.; Fischer, R. A. Organozinc ligands in transition metal chemistry. *Coord. Chem. Rev.* **2012**, *256*, 537-555. (b) Butler, M. J.; Crimmin, M. R. Magnesium, zinc, aluminium and gallium hydride complexes of the transition metals. *Chem. Commun.* **2017**, *53*, 1348-1365. For specific examples of Zn-based Z-type ligands, see: (c) Liberman-Martin, A. L.; Levine, D. S.; Ziegler, M. S.; Bergman R. G.; Tilley, T. D. Lewis acid-base interactions between platinium(II) diaryl complexes and bis(perfluorophenyl)zinc: Strongly accelerated reductive elimination induced by a Z-type ligand. *Chem. Commun.* **2016**, *52*, 7039-7042. (d) Steinhoff, P.; Steinbock, R.; Friedrich, A.; Schieweck, B. G.; Cremer, C.; Truong, K. N.; Tauchert, M. E. Synthesis and properties of heterobimetallic rhodium complexes featuring Li^{I}, Cu^{I} or Zn^{II} as a Lewis acidic metalloligand. *Dalton Trans.* **2018**, *47*, 10439-10442. (e) Steinhoff, P.; Paul, M.; Schroers, J. P.; Tauchert, M. E. Highly efficient palladium-catalysed carbon dioxide hydrosilylation employing PMP ligands. *Dalton Trans.* **2019**, *48*, 1017-1022.

(40) Schunn, R. A.; Wonchoba, E. R.; Wilkinson, G. Chlorohydridotris(triphenylphosphine)ruthenium(II). *Inorg. Synth.* **1972**, *13*, 131–134.

(41) Miloserdov, F. M.; Rajabi, N. A.; Lowe, J. P.; Mahon, M. F.; Macgregor, S. A.; Whittlesey, M. K. Zn-Promoted C-H reductive elimination and H_2 activation via a dual unsaturated heterobimetallic Ru-Zn intermediate. *J. Am. Chem. Soc.* **2020**, *142*, 6340–6349.

(42) Ahmad, N.; Levison, J. J.; Robinson, S. D.; Uttley, M. F. Tricarbonylbis(triphenylphosphine)ruthenium(0). *Inorg. Synth.* **1974**, *15*, 50-51.

(43) $Ru(PPh_3)_2(CO)_2H_2$ was characterized by comparison of the hydride chemical shifts (δ -6.34 in C_6D_6; δ -6.95 in THF-d_8) to literature data, and through independent synthesis

of the complex through photolysis of $Ru(PPh_3)_2(CO)_3$ in the presence of H_2 reported in the same paper. Sleigh, C. J.; Duckett, S. B.; Mawby, R. J.; Lowe, J. P. NMR detection of thermal and photochemical dihydrogen addition products of mon-and trinuclear ruthenium complexes containing carbonyl and triphenylphosphine ligands through para-hydrogen induced polarization. *Chem. Commun.* **1999**, 1223-1224.

(44) Douglas, T. M.; Chaplin, A. B.; Weller, A. S.; Yang, X.; Hall, M. B. Monomeric and oligomeric amine-borans σ-complexes of rhodium. Intermediates in the catalytic dehydrogenation of amine boranes. *J. Am. Chem. Soc.* **2009**, *131*, 15440-15456.

(45) Sheldrick, G. M. SHELXT - Integrated space-group and crystal structure determination. *Acta Cryst.* **2015**, *A71*, 3-8.

(46) Sheldrick, G. M. Crystal structure refinement with SHELXL. *Acta Cryst.* **2015**, *C71*, 3-8.

(47) Dolomanov, O. V.; Bourhis, L. J.; Gildea, R. J.; Howard, J. A. K.; Puschmann, H. OLEX2: A complete structure solution, refinement and analysis program. *J. Appl. Cryst.* **2011**, *42*, 339-341.

(48) Frisch, M. J.; Trucks, G. W.; Schlegel, H. B.; Scuseria, G. E.; Robb, M. A.; Cheeseman, J. R.; Scalmani, G.; Barone, V.; Mennucci, B.; Petersson, G. A.; Nakatsuji, H.; Caricato, M.; Li, X.; Hratchian, H. P.; Izmaylov, A. F.; Bloino, J.; Zheng, G.; Sonnenberg, J. L.; Hada, M.; Ehara, M.; Toyota, K.; Fukuda, R.; Hasegawa, J.; Ishida, M.; Nakajima, T.; Honda, Y.; Kitao, O.; Nakai, H.; Vreven, T.; Montgomery, J. A.; Peralta, J. E.; Ogliaro, F.; Bearpark, M.; Heyd, J. J.; Brothers, E.; Kudin, K. N.; Staroverov, V. N.; Kobayashi, R.; Normand, J.; Raghavachari, K.; Rendell, A.; Burant, J. C.; Iyengar, S. S.; Tomasi, J.; Cossi, M.; Rega, N.; Millam, J. M.; Klene, M.; Knox, J. E.; Cross, J. B.; Bakken, V.; Adamo, C.; Jaramillo, J.; Gomperts, R.; Stratmann, R. E.; Yazyev, O.; Austin, A. J.; Cammi, R.; Pomelli, C.;

Ochterski, J. W.; Martin, R. L.; Morokuma, K.; Zakrzewski, V. G.; Voth, G. A.; Salvador, P.; Dannenberg, J. J.; Dapprich, S.; Daniels, A. D.; Farkas; Foresman, J. B.; Ortiz, J. V.; Cioslowski, J.; Fox, D. J. Gaussian 09, Revision D.01, Gaussian Inc.: Wallingford CT, **2013**.

(49) Becke, A. D. Density-functional exchange-energy approximation with correct asymptotic behavior. *Phys. Rev. A* **1988**, *38*, 3098-3100.

(50) Perdew, J. P. Density-functional approximation for the correlation energy of the inhomogeneous electron gas. *Phys. Rev. B* **1986**, *33*, 8822-8824.

(51) Andrae, D.; Häußermann, U.; Dolg, M.; Stoll, H.; Preuß, H. Energy-adjusted ab initio pseudopotentials for the second and third row transition elements. *Theor. Chim. Acta* **1990**, *77*, 123-141.

(52) Hehre, W. J.; Ditchfield, R.; Pople, J. A. Self-consistent molecular orbital methods. XII. Further extensions of Gaussian-type basis sets for use in molecular orbital studies of organic molecules. *J. Chem. Physics* **1972**, *56*, 2257-2261.

(53) Hariharan, P. C.; Pople, J. A. The influence of polarization functions on molecular orbital hydrogenation energies. *Theor. Chim. Acta* **1973**, *28*, 213-222.

(54) Höllwarth, A.; Böhme, M.; Dapprich, S.; Ehlers, A. W.; Gobbi, A.; Jonas, V.; Köhler, K. F.; Stegmann, R.; Veldkamp, A.; Frenking, G. A set of d-polarization functions for pseudo-potential basis sets of the main group elements Al-Bi and f-type polarization functions for Zn, Cd, Hg. *Chem. Phys. Lett.* **1993**, *208*, 237-240.

(55) Häller, L. J. L.; Page, M. J.; Erhardt, S.; Macgregor, S. A.; Mahon, M. F.; Naser, M. A.; Vélez, A.; Whittlesey, M. K. Experimental and computational investigation of C−N bond activation in ruthenium N-heterocyclic carbene complexes. *J. Am. Chem. Soc.* **2010**, *132*, 18408-18416.

(56) Chai, J.-D.; Head-Gordon, M. Long-range corrected hybrid density functionals with damped atom–atom dispersion corrections. *Phys. Chem. Chem. Phys.* **2008**, *10*, 6615-6620.

(57) Weigend, F.; Ahlrichs, R. Balanced basis sets of split valence, triple zeta valence and quadruple zeta valence quality for H to Rn: Design and assessment of accuracy. *Phys. Chem. Chem. Phys.* **2005**, *7*, 3297-3305.

(58) Weigend, F. Accurate Coulomb-fitting basis sets for H to Rn. *Phys. Chem. Chem. Phys.* **2006**, *8*, 1057-1065.

(59) Tomasi, J.; Mennucci, B.; Cammi, R. Quantum mechanical continuum solvation models. *Chem. Rev.* **2005**, *105*, 2999-3093.

(60) Bader, R. F. W. *Atoms in Molecules: A Quantum Theory*. Clarendon Press: 1994.

(61) Keith, T. A. *AIMAll (Version 17.11.14)*, TK Gristmill Software: Overland Park KS, USA, 2017.

(62) Contreras-García, J.; Johnson, E. R.; Keinan, S.; Chaudret, R.; Piquemal, J.-P.; Beratan, D. N.; Yang, W. NCIPLOT: A program for plotting noncovalent interaction regions. *J. Chem. Theory Comput.* **2011**, *7*, 625-632.

(63) Humphrey, W.; Dalke, A.; Schulten, K. VMD: Visual molecular dynamics. *J. Mol. Graph.* **1996**, *14*, 33-38.

(64) Mitoraj, M. P.; Michalak, A.; Ziegler, T. A combined charge and energy decomposition scheme for bond analysis. *J. Chem. Theory Comput.* **2009**, *5*, 962-975.

(65) te Velde, G.; Bickelhaupt, F. M.; Baerends, E. J.; Fonseca Guerra, C.; van Gisbergen, S. J. A.; Snijders, J. G.; Ziegler, T. Chemistry with ADF. *J. Comput. Chem.* **2001**, *22*, 931-967.

(66) Glendening, E. D.; Badenhoop, J. K.; Reed, A. E.; Carpenter, J. E.; Bohmann, J. A.; Morales, C. M; Landis, C. R.; Weinhold, F. NBO 6.0, Theoretical Chemistry Institute, University of Wisconsin, Madison, WI., 2013.

(67) Chemcraft version 1.8, see http://www.chemcraftprog.com.

(68) Compound **1** is shown in Scheme 2 with dotted lines between C_{ipso}···Zn (2.360(3) Å) and Zn···Zn (2.6000(5) Å) to illustrate the presence of close contacts to the Zn centers (see Figure S1 in the Supporting Information). We appreciate the comments of one of the referees about how to represent these interactions in **1**.

(69) Ferrence, G. M.; Fanwick, P. E.; Kubiak, C. P.; Haines, R. J. High-pressure synthesis of $[Ru_2(\mu\text{-dppm})_2(\mu\text{-CO})(CO)_4]$, $[Ru_2(\mu\text{-dppm})(\mu\text{-dmpm})(\mu\text{-CO})(CO)_4]$, and $[Ru(dcypm)(CO)_3]$ from $Ru_3(CO)_{12}$ and the diphosphines: $R_2PCH_2PR_2$; R=CH_3 (dmpm), C_6H_5 (dppm) and C_6H_{11} (dcypm). Crystal and molecular structures of $[Ru_2(\mu\text{-dppm})_2(\mu\text{-CO})(CO)_4]$, and $[Ru(dcypm)(CO)_3]$. *Polyhedron* **1997**, *16*, 1453-1459.

(70) Skoog, S. J.; Jorgenson, A. L.; Campbell, J. P.; Douskey, M. L.; Munson, E.; Gladfelter, W. L. Structure and reactivity of the zero-valent ruthenium complex Ru(1,2-bis(diphenylphosphino)ethane)$(CO)_3$ and the dicationic ruthenium dimer $[Ru_2(1,2\text{-bis(diphenylphosphino)ethane})_2(CO)_6]^{2+}$. *J. Organomet. Chem.* **1998**, *557*, 13-28.

(71) Bunten, K. A.; Farrar, D. H.; Poë, A. J.; Lough, A. J. Chelation kinetics of bidentate phosphine ligands on pentacoordinate ruthenium carbonyl complexes. *Organometallics* **2000**, *19*, 3674-3682.

(72) Phanopoulos, A.; Brown, N. J.; White, A. J. P.; Long, N. J.; Miler, P. W. Synthesis, characterization, and reactivity of ruthenium hydride complexes of N-centered triphosphine ligands. *Inorg. Chem.* **2014**, *53*, 3742-3752.

(73) Angles in the two compounds are as follows; **2**: ∠C-Ru-C: 103.00(11)°, 104.99(10)°, 152.01(11)°; ∠P-Ru-P = 159.35(2) °; Ru(Xantphos)$(CO)_3$: ∠C-Ru-C: 87.62(11)°, 88.10(11)°, 149.51(12)°; ∠P-Ru-P: 101.80(2)°. The higher frequency ν(CO) bands for **2** (2012, 1959 and 1931 cm^{-1}) versus Ru(Xantphos)$(CO)_3$ (2007, 1921 and 1920 cm^{-1}) would be consistent with the removal of electron density from the Ru center by the Z-acceptor ZnPhos ligand, however the differences in structure of the two compounds makes any direct comparison less than straightforward. Ledger, A. E. W.; Slatford, P. A.; Lowe, J. P.; Mahon, M. F.; Whittlesey, M. K.; Williams, J. M. J. Ruthenium xantphos complexes in hydrogen transfer processes: Reactivity and mechanistic studies. *Dalton Trans.* **2009**, 716-722.

(74) Chan, W. H.; Zhang, Z. Z.; Mak, T. C. W.; Che, C. M. Coordination chemistry of the organometallic tridentate ligand trans-[Ru(2-$Ph_2PC_5H_4N$-P)$_2(CO)_3$] and crystal structures of metal complex derivatives. *J. Chem. Soc., Dalton Trans.* **1998**, 803-809.

(75) A previous DFT study on **I** and its heavier congeners has been published. Xu, X.; Fang, L.; Chen, Z.-X.; Yang, G.-C.; Sun, S.-L.; Su, Z.-M. Quantum chemistry studies on the Ru-M interactions and the ^{31}P NMR in [Ru$(CO)_3(Ph_2Ppy)_2(MCl_2)$] (M = Zn, Cd, Hg)]. *J. Organomet. Chem.* **2006**, *691*, 1927-1933.

(76) Cordero, B.; Gómez, V.; Platero-Prats, A. E.; Revés, M.; Echeverría, J.; Cremades, E.; Barragán, F.; Alvarez, S. Covalent radii revisited. *Dalton Trans.* **2008**, 2832-2838.

(77) Riddlestone, I. M.; Rajabi, N. A.; Lowe, J. P.; Mahon, M. F.; Macgregor, S. A.; Whittlesey, M. K. Activation of H_2 over the Ru-Zn bond in the transition metal-Lewis acid heterobimetallic species [Ru$(IPr)_2(CO)ZnEt]^+$. *J. Am. Chem. Soc.* **2016**, *138*, 11081-11084.

(78) Espinal-Viguri, M.; Varela-Izquierdo, V.; Miloserdov, F. M.; Riddlestone, I. M.;. Mahon, M. F.; Whittlesey, M. K. Heterobimetallic ruthenium-zinc complexes with

bulky N-heterocyclic carbenes: Syntheses, structures and reactivity. *Dalton Trans.* **2019**, *48*, 4176-4189.

(79) O'Leary, N.; Miloserdov, F. M.; Mahon, M. F.; Whittlesey, M. K. Transforming PPh_3 into bidentate phosphine ligands at Ru-Zn heterobimetallic complexes. *Dalton Trans.* **2019**, *48*, 14000-14009.

(80) For recent overviews of H-H and more general E-H addition across M-Z interactions, see: (a) Devillard, M.; Bouhadir, G.; Bourissou, D. Cooperation between transition metals and Lewis acids: A way to activate H_2 and E-H bonds. *Angew. Chem. Int. Ed.* **2015**, *54*, 730-732. (b) Owen, G. R. Functional group migrations between boron and metal centres within transition metal-borane and -boryl complexes and cleavage of H–H, E–H and E–E' bonds. *Chem. Commun.* **2016**, *52*, 10712-10726.

(81) For specific examples of H_2 addition across M-Z bonds, see: (a) Tsoureas, N.; Kuo, Y.-Y.; Haddow, M. F.; Owen, G. R. Double addition of H_2 to transition metal–borane complexes: A 'hydride shuttle' process between boron and transition metal centres. *Chem. Commun.* **2011**, *47*, 484-486. (b) ref 10. (c) ref 12. (d) Barnett, B. R.; Moore, C. E.; Rheingold, A. L.; Figueroa, J. S. Cooperative transition metal/Lewis acid bond-activation reactions by a bidentate (boryl)iminomethane complex: A significant metal-borane interaction promoted by a small bite-angle LZ chelate. *J. Am. Chem. Soc.* **2014**, *136*, 10262-10265. (e) Cowie, B. E.; Emslie, D. J. H. Platinum complexes of a borane-appended analogue of 1,1`-bis(diphenylphosphino)ferrocene: Flexible borane coordination modes and in situ vinylborane formation. *Chem. Eur. J.* **2014**, *20*, 16899-16912.

(82) Schott, D.; Callaghan, P.; Dunne, J.; Duckett, S. B.; Godard, C.; Goicoechea, J. M.; Harvey, J. N.; Lowe, J. P.; Mawby, R. J.; Muller, G.; Perutz, R. N.; Poli, R.; Whittlesey, M. K. The reaction of $[M(CO)_3(Ph_2PCH_2CH_2PPh_2)]$ (M = Fe, Ru) with

parahydrogen: probing the electronic structure of reaction intermediates and the internal rearrangement mechanism for the dihydride products. *Dalton Trans.* **2004**, 3218-3224.

(83) Vance, J. R.; Schäfer, A.; Robertson, A. P. M.; Lee, K.; Turner, J.; Whittell, G. R.; Manners, I. Iron-catalyzed dehydrocoupling/dehydrogenation of amine-boranes. *J. Am. Chem. Soc.* **2014**, *136*, 3048-3064.

(84) No attempt was made to determine the fate of the zinc atom.

(85) Other examples of E-$C_6H_4PR_2$ bond cleavage have been reported in which the E group is retained in the metal coordination sphere. (a) E = Si, R= Cy: Mitton, S. J.; McDonald, R.; Turculet, L. Nickel and palladium silyl pincer complexes: Unusual structural rearrangements that involve reversible Si-C(sp^3) and Si-C(sp^2) bond activation. *Angew. Chem. Int. Ed.* **2009**, *48*, 8568-8571. (b) E = Ge, R= Cy: Kameo, H.; Ishii, S.; Nakazawa, H. Facile synthesis of rhodium and iridium complexes bearing a [PEP]-type ligand (E = Ge or Sn) via E-C bond cleavage. *Dalton Trans.* **2012**, *41*, 11386-11392.

(86) Davies, C. J. E.; Lowe, J. P.; Mahon, M. F.; Poulten, R. C.; Whittlesey, M. K. Synthesis and small molecule reactivity of trans-dihydride isomers of $Ru(NHC)_2(PPh_3)_2H_2$ (NHC = N-heterocyclic carbene). *Organometallics* **2013**, *32*, 4927-4937.

(87) QTAIM studies on **3** showed no direct Ru-Zn bond path with bonding being diverted through the bridging hydrides. See Figure S33.

(88) Rajabi, N. A. Ph.D. Thesis, Heriot-Watt University, 2018.

(89) This is also confirmed by NBO analyses. See Figure S31.

(90) Adams, G. M.; Weller, A. S. POP-type ligands: Variable coordination and hemilabile behavior. *Coord. Chem. Rev.* **2018**, *355*, 150-172.

(91) QTAIM identifies Ru-Zn bond paths in each case with BCP ρ(r) values ranging from 0.038 to 0.048 au. The case of Ru(2-$Ph_2PC_5H_4N)_2(CO)_3(ZnCl_2)$ (**I**, Scheme 3) has also been considered for completeness (Figure S30).

(92) Ogasawara, M.; Macgregor, S. A.; Streib, W. E.; Folting, K.; Eisenstein, O.; Caulton, K. G. Isolable, unsaturated Ru(0) in $Ru(CO)_2(P^tBu_2Me)_2$: Not isostructural with Rh(I) in $Rh(CO)_2(PR_3)_2^+$. *J. Am. Chem. Soc.* **1995**, *117*, 8869-8870.

(93) Ogasawara, M.; Macgregor, S. A.; Streib, W. E.; Folting, K.; Eisenstein, O.; Caulton, K. G. Characterization and reactivity of an unprecedented unsaturated zero-valent ruthenium species: Isolable, yet highly reactive. *J. Am. Chem. Soc.* **1996**, *118*, 10189-10199.

(94) The formation of **3** + CO from **2** + H_2 is thermodynamically uphill by 3.5 kcal/mol. However, under the experimental conidtions, we assume rapid reaction with H_2 upon loss of CO from **2** and that this is irreversible, the barrier for H_2 reductive elimination from **3** being 26.9 kcal/mol.

(95) Jean, Y. *Molecular orbitals of transition metal complexes*; Oxford University Press: Oxford, **2005**.

(96) Hopkinson, M. N.; Richter, C.; Schedler, M.; Glorius, F. An overview of N-heterocyclic carbenes. *Nature* **2014**, *510*, 485-496.

(97) Flügel, R.; Windmüller, B.; Gevert, O.; Werner, H. Synthesis, molecular structure and reactions of stable square-planar 16-electron ruthenium(0) complexes. *Chem. Ber.* **1996**, *129*, 1007-1013.

(98) Gottschalk-Gaudig, T.; Huffman, J. C.; Caulton, K. G.; Gérard, H.; Eisenstein, O. Solution and solid-state structure of $Ru(CO)_2(^tBu_2PC_2H_4P^tBu_2)$: Square planar and monomeric? *J. Am. Chem. Soc.* **1999**, *121*, 3242-3243.

(99) Gottschalk-Gaudig, T.; Huffman, J. C.; Gérard, H.; Eisenstein, O.; Caulton, K. G. Unsaturated Ru(0) species with a constrained bis-phosphine ligand: $[Ru(CO)_2(^tBu_2PCH_2CH_2P^tBu_2)]_2$. Comparison to $[Ru(CO)_2(P^tBu_2Me)_2]$. *Inorg. Chem.* **2000**, *39*, 3957-3962.

(100) Calculations with the CAM-B3LYP functional provided good agreement with the experimental spectrum. See Figure S38.

(101) Hall, C.; Jones, W. D.; Mawby, R. J.; Osman, R. Perutz, R. N.; Whittlesey, M. K. Matrix isolation and transient photochemistry of ruthenium complex $Ru(dmpe)_2H_2$; Characterization and reactivity of $Ru(dmpe)_2$ (dmpe = $Me_2PCH_2CH_2PMe_2$). *J. Am. Chem. Soc.* **1992**, *114*, 7425-7435.

(102) Fogler, E.; Iron, M. A.; Zhang, J.; Ben-David, Y.; Diskin-Posner, Y.; Leitus, G.; Shimon, L.W.; Milstein, D. Ru(0) and Ru(II) nitrosyl pincer complexes: Structure, reactivity, and catalytic activity. *Inorg. Chem.* **2013**, *52*, 11469-11479.

TOC Graphic and Text

The preparation of Ru(ZnPhos)$(CO)_3$ (**2**) and Ru(ZnPhos)$(IMe_4)_2$ (**4**) featuring the novel ZnPhos ligand (ZnPhos = Zn(o-$C_6H_4PPh_2)_2$) is described. Under photolysis **2** adds H_2 across the Ru-Zn bond to form Ru(ZnPhos)$(CO)_2(\mu\text{-}H)_2$ (**3**); in contrast, **4** adds H_2 reversibly at Ru to give Ru(ZnPhos)$(IMe_4)_2H_2$ (**5**). DFT calculations rationalize these differences and characterize the Ru→Zn interactions in these species. **4** can be considered a Zn-stabilized Ru(0)L_4 species that is, unusually, devoid of strong π-acceptor ligands.